

NASA TECHNICAL NOTE



NASA TN D-3461

c 1

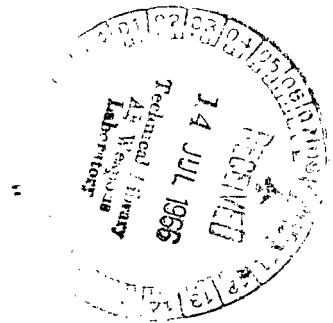
NASA TN D-3461

LOAN COPY: RE
AFWL (WL)
KIRTLAND AFB,



A THEORETICAL ANALYSIS OF THE DYNAMIC LATERAL STABILITY AND CONTROL OF A PARAWING VEHICLE

by Joseph R. Chambers and Peter C. Boisseau
Langley Research Center
Langley Station, Hampton, Va.



TECH LIBRARY KAFB, NM



0130365

NASA TN D-3461

**A THEORETICAL ANALYSIS OF THE DYNAMIC LATERAL STABILITY
AND CONTROL OF A PARAWING VEHICLE**

By Joseph R. Chambers and Peter C. Boisseau

**Langley Research Center
Langley Station, Hampton, Va.**

NATIONAL AERONAUTICS AND SPACE ADMINISTRATION

For sale by the Clearinghouse for Federal Scientific and Technical Information
Springfield, Virginia 22151 - Price \$2.00

A THEORETICAL ANALYSIS OF THE DYNAMIC LATERAL STABILITY AND CONTROL OF A PARAWING VEHICLE*

By Joseph R. Chambers and Peter C. Boisseau
Langley Research Center

SUMMARY

A theoretical analysis has been made to provide an understanding of some of the fundamentals of the dynamic lateral stability and control of parawing vehicles. The analysis is treated mainly in terms of the effects of vertical center-of-gravity position, since this factor is responsible for most of the unusual characteristics of such vehicles.

Increasing the vertical distance between the payload and parawing led to decreased damping of the roll-subsidence mode and increased damping of the spiral mode. It also caused an increase in the damping and period of the lateral oscillation and a reduction in the ratio of roll to sideslip. The stability derivative C_{np} (yawing-moment coefficient due to rolling angular velocity) and the mass parameter K_{XZ} (nondimensional product-of-inertia parameter) were found to be the principal factors influencing the damping of the lateral oscillation as the center-of-gravity location was lowered with respect to the parawing.

There was little effect of vertical center-of-gravity location on the initial roll response to wing bank control but as the motion progressed, the configurations having the lower center-of-gravity locations displayed the greater roll response. The effects of vertical center-of-gravity location on the mass distribution of the system produced significant changes in the initial yawing motion following the application of wing bank control. It was found that the large nose-down inclination of the principal axis of least inertia caused by lowering the center-of-gravity position relative to the parawing tended to reduce the initial adverse yawing motion of the system.

INTRODUCTION

Recently, the National Aeronautics and Space Administration has been conducting general investigations to provide some fundamental information on the stability and control characteristics of parawing configurations. (See refs. 1 to 4, for example.) The present investigation has been made to improve the basic understanding of the dynamic lateral stability and control of parawing configurations. The characteristics of such

*The material presented herein includes information from a thesis entitled "An Investigation of the Dynamic Lateral Stability and Control of a Parawing Vehicle" by Joseph R. Chambers submitted to Virginia Polytechnic Institute, Blacksburg, Va., May 1966 in partial fulfillment of the requirements for the degree of Master of Science.

configurations would be expected to differ from those of conventional aircraft in significant ways because certain physical characteristics of the configurations which are important to dynamic stability differ markedly from the characteristics of conventional aircraft. These physical characteristics are: (1) a center-of-gravity location far below the wing, (2) a mass distribution in which the mass is distributed mainly along the vertical axis, and (3) a wing having a shape which tends to give unusually large values of lateral force due to sideslip. The second factor is a consequence of the first, and the third factor is important because of the first. Consequently, since the low center-of-gravity position was expected to be the principal cause of differences in stability of the parawing configuration from conventional aircraft, the investigation of stability is treated mainly in terms of the effect of vertical center-of-gravity location on lateral stability. The effects of individual stability derivatives were also investigated to determine those that were of predominant importance and to determine those that, in changing as the vertical location of the center of gravity was changed, were primarily responsible for the effects of center-of-gravity location on dynamic lateral stability.

The investigation consisted of a theoretical determination of the dynamic lateral characteristics of an unpowered parawing-payload combination gliding at maximum lift-drag ratio for several vertical center-of-gravity locations. Stability derivatives used in the calculations were based on the results of static- and dynamic-force tests of a parawing model having an aspect ratio of 2.83 and a deployed leading-edge sweep angle of 50°. The effects of center-of-gravity location on these stability derivatives are considered important in themselves to the understanding of the dynamic stability and control of parawing vehicles. Consequently, the effects of center-of-gravity location on the stability derivatives are analyzed as a distinct part of the investigation.

SYMBOLS AND NOMENCLATURE

The calculated stability and control results are presented with respect to the stability axis system shown in figure 1. All basic force test data of the parawing model are presented for the body axis system shown in figure 2. The aerodynamic coefficients are based on the flat-pattern characteristics of the parawing (45° leading-edge sweep condition). Indicated dimensional units are given first in the International System (SI) and parenthetically in U.S. Customary System of Units.

A,B,C,D,E	coefficients of lateral stability quartic
b	wing span, meters (feet)
\bar{c}	mean aerodynamic chord, meters (feet)

C_D	drag coefficient, $F_D/q_\infty S$
C_L	lift coefficient, $F_L/q_\infty S$
C_l	rolling-moment coefficient, $M_X/q_\infty S b$
ΔC_l	incremental rolling-moment coefficient
C_m	pitching-moment coefficient, $M_Y/q_\infty S \bar{c}$
C_n	yawing-moment coefficient, $M_Z/q_\infty S b$
ΔC_n	incremental yawing-moment coefficient
C_Y	side-force coefficient, $F_Y/q_\infty S$
ΔC_Y	incremental side-force coefficient
$C_{1/2}$	number of cycles required for amplitude of a lateral oscillation to decrease by a factor of 2
D_b	differential operator, d/ds_b
f	frequency of oscillation, cycles per second
F_D	drag, newtons (pounds)
F_L	lift, newtons (pounds)
F_Y	side force, newtons (pounds)
g	acceleration due to gravity, meters/second ² (feet/second ²)
k	reduced frequency parameter, $\frac{\omega b}{2V}$
k_{X_0}	radius of gyration in roll about principal longitudinal axis, meters (feet)
k_{Z_0}	radius of gyration in yaw about principal vertical axis, meters (feet)

K_{X_0}	nondimensional radius of gyration in roll about principal longitudinal axis, k_{X_0}/b
K_{Z_0}	nondimensional radius of gyration in yaw about principal vertical axis, k_{Z_0}/b
K_X	nondimensional radius of gyration in roll about longitudinal stability axis, $\sqrt{K_{X_0}^2 \cos^2 \eta + K_{Z_0}^2 \sin^2 \eta}$
K_Z	nondimensional radius of gyration in yaw about vertical stability axis, $\sqrt{K_{X_0}^2 \sin^2 \eta + K_{Z_0}^2 \cos^2 \eta}$
K_{XZ}	nondimensional product-of-inertia parameter, $(K_{Z_0}^2 - K_{X_0}^2) \sin \eta \cos \eta$
L/D	lift-drag ratio
$(L/D)_{\max}$	maximum lift-drag ratio
m	mass, kg (slugs)
M_X	rolling moment, meter-newton (foot-pound)
M_Y	pitching moment, meter-newton (foot-pound)
M_Z	yawing moment, meter-newton (foot-pound)
P	period of oscillation, second
p	rolling velocity, radians/second
q_∞	free-stream dynamic pressure, newton/square meter (pound/square foot)
r	yawing velocity, radians/second
S	wing area, square meter (square foot)
s_b	nondimensional time parameter based on span, Vt/b

t	time, second
$t_{1/2}$	time required for amplitude of lateral oscillation to decrease by a factor of 2, second
V	free-stream velocity, meters/second (feet/second)
$v_e = V \sqrt{\sigma} \sin \beta \approx V \sqrt{\sigma} \beta$	
X,Y,Z	body reference axes
$\frac{x}{b}, \frac{z}{b}$	nondimensional distances along the body reference axes measured from basic moment reference center (see fig. 3)
\bar{x}, \bar{z}	nondimensional distances measured from 0.5 keel length station to center-of-gravity location measured in axis system parallel to stability axes (see fig. 1)
x_i	any of mass or aerodynamic terms in lateral equations of motion
α	angle of attack of keel, degrees
β	angle of sideslip, degrees or radians
$\dot{\beta}$	rate of change of sideslip, radians/second
β_w	angle of sideslip of parawing, degrees
ϵ	angle between reference axis and principal axis, positive when reference axis is above principal axis at nose, degree (see fig. 1)
η	angle of attack of principal longitudinal axis, positive when principal axis is above flight path at nose, degree (see fig. 1)
γ	flight-path angle, degree (see fig. 1)
λ	root of stability quartic $A\lambda^4 + B\lambda^3 + C\lambda^2 + D\lambda + E = 0$
μ_b	lateral relative-density factor, $m/\rho S b$

ϕ	angle of bank, degrees or radians
ϕ_w	angle of bank of parawing, positive when right wing tip is down, degree
σ	ratio of air density at altitude to that at sea level
ψ	angle of yaw, degrees or radians
$\left \frac{\phi}{\psi} \right $	ratio of amplitudes of roll and yaw present in a mode of motion
$\left \frac{\phi}{\beta} \right $	ratio of amplitudes of roll and sideslip present in a mode of motion
$\left \frac{\phi}{v_e} \right $	ratio of bank-angle amplitude to equivalent-side-velocity amplitude for oscillatory mode, $\left \frac{\phi}{\beta} \right \frac{57.3}{V\sqrt{\sigma}}, \frac{\text{deg}}{\text{m/sec}} \left(\frac{\text{deg}}{\text{ft/sec}} \right)$
ρ	mass density of air, kilograms/cubic meter (slugs/cubic foot)

$$\omega = 2\pi f, \text{ radians/second}$$

$$C_{l\beta} = \frac{\partial C_L}{\partial \beta}, \text{ per degree or per radian}$$

$$C_{n\beta} = \frac{\partial C_n}{\partial \beta}, \text{ per degree or per radian}$$

$$C_{Y\beta} = \frac{\partial C_Y}{\partial \beta}, \text{ per degree or per radian}$$

$$C_{lp} = \frac{\partial C_L}{\partial \frac{pb}{2V}}$$

$$C_{np} = \frac{\partial C_n}{\partial \frac{pb}{2V}}$$

$$C_{Yp} = \frac{\partial C_Y}{\partial \frac{pb}{2V}}$$

$$C_{l\dot{p}} = \frac{\partial C_L}{\partial \frac{\dot{p}b^2}{4V^2}}$$

$$C_{n\dot{p}} = \frac{\partial C_n}{\partial \frac{\dot{p}b^2}{4V^2}}$$

$$C_{Y\dot{p}} = \frac{\partial C_Y}{\partial \frac{\dot{p}b^2}{4V^2}}$$

$$C_{l_r} = \frac{\partial C_l}{\partial \frac{rb}{2V}}$$

$$C_{n_r} = \frac{\partial C_n}{\partial \frac{rb}{2V}}$$

$$C_{Y_r} = \frac{\partial C_Y}{\partial \frac{rb}{2V}}$$

$$C_{l_{\dot{r}}} = \frac{\partial C_l}{\partial \frac{\dot{rb}^2}{4V^2}}$$

$$C_{n_{\dot{r}}} = \frac{\partial C_n}{\partial \frac{\dot{rb}^2}{4V^2}}$$

$$C_{Y_{\dot{r}}} = \frac{\partial C_Y}{\partial \frac{\dot{rb}^2}{4V^2}}$$

$$C_{l_{\dot{\beta}}} = \frac{\partial C_l}{\partial \frac{\dot{\beta}b}{2V}}$$

$$C_{n_{\dot{\beta}}} = \frac{\partial C_n}{\partial \frac{\dot{\beta}b}{2V}}$$

$$C_{Y_{\dot{\beta}}} = \frac{\partial C_Y}{\partial \frac{\dot{\beta}b}{2V}}$$

Dots over symbols denote derivatives with respect to time.

In the present investigation the term "in-phase derivative" refers to any one of the oscillatory derivatives that is based on the components of forces and moments in phase with the angular displacement during the oscillatory tests. The term "out-of-phase derivative" refers to any one of the stability derivatives that is based on the components of forces and moments 90° out of phase with angular displacement. The oscillatory derivatives of the present investigation were measured in the following combinations:

Rolling oscillation tests:

$$\left. \begin{array}{l} C_{l_{\beta}} \sin \alpha - k^2 C_{l_{\dot{\beta}}} \\ C_{n_{\beta}} \sin \alpha - k^2 C_{n_{\dot{\beta}}} \\ C_{Y_{\beta}} \sin \alpha - k^2 C_{Y_{\dot{\beta}}} \end{array} \right\} \text{In phase}$$

$$\left. \begin{array}{l} C_{l_p} + C_{l_{\dot{\beta}}} \sin \alpha \\ C_{n_p} + C_{n_{\dot{\beta}}} \sin \alpha \\ C_{Y_p} + C_{Y_{\dot{\beta}}} \sin \alpha \end{array} \right\} \text{Out of phase}$$

Yawing oscillation tests:

$$\begin{array}{l}
 C_{l_{\beta}} \cos \alpha + k^2 C_{l_{\dot{\beta}}} \\
 C_{n_{\beta}} \cos \alpha + k^2 C_{n_{\dot{\beta}}} \\
 C_{Y_{\beta}} \cos \alpha + k^2 C_{Y_{\dot{\beta}}}
 \end{array}
 \left. \vphantom{\begin{array}{l} C_{l_{\beta}} \cos \alpha + k^2 C_{l_{\dot{\beta}}} \\ C_{n_{\beta}} \cos \alpha + k^2 C_{n_{\dot{\beta}}} \\ C_{Y_{\beta}} \cos \alpha + k^2 C_{Y_{\dot{\beta}}} \end{array}} \right\} \text{In phase}$$

$$\begin{array}{l}
 C_{l_r} - C_{l_{\dot{\beta}}} \cos \alpha \\
 C_{n_r} - C_{n_{\dot{\beta}}} \cos \alpha \\
 C_{Y_r} - C_{Y_{\dot{\beta}}} \cos \alpha
 \end{array}
 \left. \vphantom{\begin{array}{l} C_{l_r} - C_{l_{\dot{\beta}}} \cos \alpha \\ C_{n_r} - C_{n_{\dot{\beta}}} \cos \alpha \\ C_{Y_r} - C_{Y_{\dot{\beta}}} \cos \alpha \end{array}} \right\} \text{Out of phase}$$

METHOD OF ANALYSIS

The analysis was made for a hypothetical paraglider system consisting of a parawing-payload combination having the mass characteristics of a recently proposed recovery system. The parawing and payload were assumed to be rigidly joined so that there was no relative motion between them except for intentional control movements. Longitudinal trim was assumed to be obtained solely by varying the fore-and-aft position of the center of gravity of the system. The vertical center-of-gravity location was varied by locating the payload relative to the parawing in such a manner as to yield several specified center-of-gravity locations perpendicular to the parawing keel member (in terms of z/b) while maintaining the proper position parallel to the keel (in terms of x/b) required for longitudinal trim. The stability derivatives for each center-of-gravity location were then estimated from measured derivatives for the wing alone, and calculations were made to determine the dynamic lateral stability and control of the vehicle for each center-of-gravity location.

Description of Vehicle

The recovery system was assumed to employ an aspect-ratio-2.83 parawing having a conical canopy and flat-pattern sweep angle of 45° . In the deployed or flight condition, the parawing fabric was supported in a 50° sweep condition by three rigid tubular members which formed the keel and leading edges of the parawing. Parawing and payload

weights were 1779 newtons (400 pounds) and 15 124 newtons (3400 pounds), respectively. Wing loading was 337 newtons per square meter (7.04 pounds per square foot). The payload aerodynamics were assumed to consist only of drag and were considered only in the determination of longitudinal trim. The system center-of-gravity location was varied in the previously discussed manner such that three different configurations of the original concept were studied. These configurations are herein referred to as A, B, and C ($\frac{z}{b} = 0.25, 0.50, \text{ and } 0.75, \text{ respectively}$).

The configurations were assumed to use the wing-bank system for lateral control; that is, the wing was banked about an axis parallel to the keel member to produce the forces and moments required for lateral control. This control system is, in effect, similar to the center-of-gravity shift type of control actually used on parawings with suspended payloads. As stated in reference 3, when such a system is used for control the incremental lateral force and moment coefficients produced by wing bank may approximately be expressed as

$$\left. \begin{aligned} \Delta C_Y &= C_{Y\beta} \beta_w + C_L \sin \phi_w \\ \Delta C_n &= C_{n\beta} \beta_w + \frac{\bar{x}}{b} C_L \sin \phi_w \\ \Delta C_l &= C_{l\beta} \beta_w + \frac{\bar{z}}{b} C_L \sin \phi_w \end{aligned} \right\} \quad (1)$$

where $\sin \beta_w = \sin \alpha \sin \phi_w$.

The first terms of the right-hand side of the equations arise from the fact that a value of sideslip is obtained at the parawing when the wing is banked for keel angles of attack other than zero. The second terms are the contributions of the lateral component of the lift vector which has been tilted by banking the wing.

Determination of Stability Derivatives

The lateral stability derivatives of the configurations were assumed to be due to the parawing alone. There was however virtually no information available on the dynamic stability derivatives; therefore, in order to provide reasonable inputs for the dynamic stability analysis, an experimental investigation was conducted to determine both the static and dynamic stability derivatives of a 0.15-scale model of the parawing assumed for the theoretical analysis.

A sketch of the model parawing is shown in figure 3 and the geometric characteristics are listed in table I. The model was constructed of nonporous plastic membrane attached to three equal length rigid members such that in the deployed or flight condition, the rigid members supported the fabric in a 50° sweep condition. Additional information pertaining to the model can be found in reference 5.

The static- and dynamic-force tests were conducted in a low-speed tunnel with a 12-foot octagonal test section at the Langley Research Center. The tests were made at a dynamic pressure of 78.1 newtons per square meter (1.63 pounds per square foot) which corresponds to a Reynolds number of 0.99×10^6 based on keel length. The static lateral tests were made for an angle of sideslip range of $\pm 5^\circ$. Forced oscillation tests were made in yaw and roll with angular amplitudes of $\pm 5^\circ$ and for a value of the reduced frequency parameter k of 0.25. A detailed description of the dynamic-force test equipment and the method of obtaining the dynamic parameters is presented in reference 6. The moments were all measured about the basic moment center shown in figure 3; and the static and dynamic lateral stability derivatives of the complete configurations were obtained by transferring these measured wing-alone model data to the required center-of-gravity locations by means of the equations of reference 7 which are included in appendix A of this paper for convenience.

Method and Scope of Calculations

Calculations were made to determine the dynamic lateral stability and control of the three parawing configurations for the condition of $(L/D)_{\max}$ gliding flight at an altitude of 3048 meters (10 000 feet).

The lateral stability calculations consisted of the determination of the damping and period of the lateral modes of motion. The damping of both the oscillatory and aperiodic modes is expressed in terms of the damping factor $\frac{1}{t_{1/2}}$, the reciprocal of the time to damp to one-half amplitude. Positive values of this parameter indicate stability (positive damping) and negative values indicate instability (negative damping). The calculations were made with the use of the equations of motion given in appendix B.

Calculations were also made to determine the aerodynamic and mass parameters that affected the lateral stability of the configurations to the greatest extent as the center-of-gravity location was varied. These calculations were made by the method of reference 8 which is based on a Taylor's series expansion of the roots of the stability quartic near the original solution. Although strictly applicable only for small incremental changes in derivatives and mass parameters near the original solution, the method does afford an insight into the important terms in the equations of motion as the center of gravity, and hence the stability derivatives and mass distribution are changed. The

results are presented as slopes indicating the rate of change of the damping and frequency of the various modes of the lateral motion with changes in any of the parameters in the equations of motion. In an attempt to provide a better understanding of the magnitude of the factors causing the effects of vertical center-of-gravity position shown by comparison of the results for configurations A, B, and C, additional calculations were made for configuration A in which the values of mass and aerodynamic parameters were changed one at a time to the values for configuration B to determine the effects of these individual parameter changes on damping and period.

The lateral control calculations consisted of calculation of the lateral motions following a step input of 5° wing bank angle. These calculations were made with a digital computer and used the basic equations of motion of appendix B together with control inputs calculated from equations (1).

RESULTS AND DISCUSSION

The results of the parawing model force tests are presented in figures 4 to 7. Calculated lateral stability derivatives and mass characteristics of the three full-scale configurations are presented in figures 8 and 9 and are given in table II. The results of the dynamic lateral stability and control calculations are presented in figures 10 to 14, the sensitivity of the dynamic lateral stability of the configurations to changes in the stability derivatives and mass parameters being given in tables III and IV. The two primary results of the investigation – the changes in the stability derivatives and mass parameters with center-of-gravity location and the effects on dynamic lateral stability and control of these parameter changes – are discussed separately.

It should be noted that any theoretical analysis of the dynamics of a parawing configuration can be limited by the concept itself. The flexibility of the parawing, the means of connection between parawing and payload, and the number of degrees of freedom of the system all complicate and in some cases may render useless any analytic attempt to predict the dynamics of the system. Consequently, the calculated results contained herein do not apply directly to parawing configurations or flight conditions other than those investigated. It is believed, however, that the major results and trends shown by these calculations are indicative of the dynamic characteristics to be expected of vehicles which have the following characteristics: very low center-of-gravity location, mass distributed mainly along the vertical axis, and a wing which has a large value of the lateral-force derivative $C_{Y\beta}$. These characteristics are typical of a wide variety of paragliders or gliding parachutes.

Stability Derivatives and Mass Parameters

Mass distribution.- The calculated mass and geometric characteristics of the three configurations are given in table II. It should be noted that for all three configurations, the nondimensional radius of gyration in roll K_X was larger than the nondimensional radius of gyration in yaw K_Z . This situation is very different from that of a conventional airplane where the radius of gyration in roll is less than that in yaw $K_X < K_Z$ and leads to near-vertical inclinations of the principal axis of least inertia. This difference would be expected to lead to substantial differences in the character of the lateral motions between parawing vehicles and conventional aircraft. For example, the large values of inclination of the axis of least inertia will lead to increased yawing components in the lateral modes of motion since a vehicle will inherently tend to move about an axis of least inertia.

It should be noted that in the present investigation the principal longitudinal axis (the axis to which η is referenced) was considered, in the conventional manner, to be the axis located in a generally forward direction. The only unusual situation was that for the parawing vehicles this axis was the one of greatest inertia.

Longitudinal characteristics.- The parawing system was assumed (on the basis of the model force-test data of fig. 4 with an added drag increment to account for the payload) to have a maximum L/D value of 4.27 at a keel angle of attack of 25° for all center-of-gravity locations. The longitudinal stability of the configurations was not investigated in this study, but it might be noted that a paraglider configuration becomes more stable longitudinally for increasing values of x/b and z/b .

Static lateral stability derivatives.- The static lateral stability characteristics of the parawing model are presented in figure 5 in the form of the static stability derivatives $C_{Y\beta}$, $C_{n\beta}$, and $C_{l\beta}$ plotted against angle of attack. The values of the derivatives were obtained from the differences between the values of the coefficients at sideslip angles of 5° and -5° . The variation of $C_{n\beta}$ (referenced to body axes) shows a negative, or destabilizing trend at an angle of attack of about 33° . It should not be inferred from this result that a vehicle with this parawing would experience a directional divergence at these higher angles of attack. It is a well-established fact that when an aircraft has large negative values of $C_{l\beta}$ in conjunction with the negative values of $C_{n\beta}$, a directional divergence does not necessarily occur. This point is discussed in detail in reference 9.

The values of the static lateral stability derivatives (referenced to stability axes) for the three configurations based on the model data and the transfer equations of the appendix are given in figure 8(a). Lowering the center-of-gravity location from configuration A to that of configuration C increased the values of both $C_{n\beta}$ and $-C_{l\beta}$. The

increase in the directional stability derivative $C_{n\beta}$ is caused by the fact that as vertical center-of-gravity location \bar{z}/b is increased, the horizontal location \bar{x}/b must also be changed to maintain longitudinal trim.

Dynamic lateral stability derivatives.- The variation of the lateral in-phase oscillatory derivatives with angle of attack for the parawing model is presented in figure 6. Static data referenced to body axes are also presented and are shown to be generally in good agreement with the oscillatory data.

The variation of the out-of-phase derivatives with angle of attack is presented in figure 7. The damping-in-roll parameter $C_{l_p} + C_{l_{\dot{\beta}}} \sin \alpha$ and the damping-in-yaw parameter $C_{n_r} - C_{n_{\dot{\beta}}} \cos \alpha$ were essentially constant over the angle-of-attack range up to the stall, which probably indicates that the $\dot{\beta}$ portion of the derivatives were negligible in the angle-of-attack range below about 35° . This apparent lack of $\dot{\beta}$ derivatives is in contrast with results of forced oscillation tests of swept rigid wings (see ref. 10, for example) in which separated flow effects have led to large values of the $\dot{\beta}$ derivatives at high angles of attack. The contrasting characteristics of the parawing may have been caused by the flexibility of the parawing itself or by leading-edge characteristics. In any event, it was assumed that the rate of change of sideslip ($\dot{\beta}$) derivatives were negligible and the measured combinations were treated as pure rolling and yawing derivatives in the dynamic stability calculations. For example, the combination $C_{l_p} + C_{l_{\dot{\beta}}} \sin \alpha$ was assumed to be C_{l_p} for purposes of determining the lateral stability derivatives of the full-scale configuration.

The calculated effect of center-of-gravity location on the dynamic lateral stability derivatives of the three full-scale parawing configurations is shown in figures 8(b) and 8(c). Lowering the center-of-gravity location from that of configuration A to configuration C led to a positive increase in the yawing moment due to rolling velocity C_{n_p} and negative increases in the damping-in-roll derivative C_{l_p} and the damping-in-yaw derivative C_{n_r} . The changes in the dynamic stability derivatives with vertical center-of-gravity location are very large because of the combination of large distance between the center of gravity and the wing and large lateral-force derivative $C_{Y_{\beta}}$ which enter into the transfer of these derivatives as products. In effect, increasing the vertical distance between the center of gravity and the parawing keel essentially makes the parawing act as a high vertical tail (with short tail length) would on a conventional airplane - that is, the side-force derivative $C_{Y_{\beta}}$ of the parawing tends to be the predominant contributor to the derivative transfer equations.

Dynamic Lateral Stability and Control

The results of the calculations to determine dynamic lateral stability are discussed in terms of the stability of the different modes of lateral motion. For conventional aircraft, these modes are usually a highly damped aperiodic rolling motion known as the roll-subsidence mode, a lightly damped aperiodic motion involving yawing and rolling known as the spiral mode, and a lateral oscillation involving yawing, rolling, and side-slipping known as the Dutch roll. Although the lateral modes of a parawing configuration may be slightly different in nature in comparison with conventional aircraft modes, the conventional nomenclature will be used to identify the various modes.

Roll-subsidence mode.- The calculated damping factor of the roll-subsidence mode of the configurations is presented in figure 10. The data indicate that the system became less damped as the center-of-gravity location of the system was moved downward from that of configuration A to that of configuration C. The dashed line represents the classical single-degree-of-freedom approximation to the roll-subsidence mode damping

$$\left(\frac{1}{t_{1/2}} = \frac{C_{lp} V}{1.57 \mu_b K_X^2 b} \right) \text{ which generally gives a reasonably accurate approximation for}$$

conventional aircraft. Comparison of the two results indicates large differences between the complete three-degree-of-freedom results and the simple single-degree-of-freedom results. This result indicates that the damping of this mode of motion is dependent on factors other than those included in the simple approximation.

The calculated variation in the damping factor of the roll-subsidence mode with changes in the various parameters in the equations of motion are presented in table III.

Positive values of $\frac{\partial \frac{1}{t_{1/2}}}{\partial x_i}$ together with positive increases in x_i (or negative values of $\frac{\partial \frac{1}{t_{1/2}}}{\partial x_i}$ together with negative increases in x_i) lead to positive (stabilizing) increases in the damping of this particular mode of motion. The results show that the yawing-moment derivatives and inertia parameters can appreciably affect the damping of this mode. The results of the additional calculations in which the parameters in the equations of motion of configuration A were changed one at a time to those of configuration B in an effort to determine the relative magnitude of the changes in the roll-mode damping due to changes in mass and aerodynamic parameters are presented in table IV together with results predicted by the slope method. The results show that the decrease in damping of the roll mode as the center-of-gravity location changed from that of configuration A to configuration B was caused primarily by the destabilizing contributions of

the derivative C_{np} and the mass parameter K_X^2 . The increased importance of the yawing derivatives in the determination of the damping of the roll mode can be explained by the data of figure 11 which presents the ratio of roll to yaw amplitude in the roll mode. Values of this parameter usually are in the range of 30 to 100 for conventional aircraft but for these parawing configurations with their associated stability parameters, all values were below 5 and indicate that the mode was not a pure rolling motion but involved relatively large yawing motions. In fact, for the lower center-of-gravity location (configuration C), the motion consisted of almost an equal rolling and yawing – which is very different from the case for conventional aircraft where the motion is almost pure rolling.

Spiral mode.– The calculated results presented in figure 10 indicate that the spiral mode became slightly more damped as the center of gravity was lowered with respect to the wing. An inspection of table IV indicates that the stabilizing effect was primarily due to the stabilizing influence of changes in those derivatives ($C_{l\beta}$ and C_{nr}) that usually affect the spiral stability of an aircraft. The spiral root can usually be approximated by $\lambda = -\frac{E}{D}$ and those terms which most affect this ratio are seen to be of great importance in the damping of the spiral mode for the parawing configuration – as they have traditionally been for conventional airplanes.

Oscillatory mode.– Presented in figure 12 is a summary of the Dutch roll oscillation characteristics of the three configurations. The inverse cyclic damping $\frac{1}{C_{1/2}}$ and roll-to-sideslip parameter $\left|\frac{\phi}{v_e}\right|$ for each configuration are presented together with the recommended boundary of reference 11 in figure 12(a). The presentation of the Dutch roll characteristics in this manner is not necessarily meant to imply that parawing configurations should conform to the handling-quality parameters of conventional aircraft, but it is one of the present standards available for evaluating the effect of the Dutch roll characteristics on flying qualities and is consequently used for purposes of comparison. The results are also compared with the older handling-quality requirements (expressed in terms of damping and period of the oscillation) of reference 12 inasmuch as the present-day aircraft requirements tend to present pessimistic views of the oscillatory characteristics of vehicles having extremely light wing loadings. (The equivalent side velocity v_e of such vehicles is much smaller than that of conventional aircraft.) The results indicate that increasing the vertical distance between parawing and payload (varying center-of-gravity location from configurations A to C) led to a longer period, better damped lateral oscillation, and smaller values of roll-to-sideslip ratio. Only configuration C satisfied the present-day handling-quality requirements, both configurations A and B lacking satisfactory Dutch roll damping. The results presented in figure 12(b) show that only configuration A did not satisfy the older handling-quality requirements.

Tables III and IV indicate that the increase in damping as the center of gravity is lowered is primarily caused by the stabilizing contribution resulting from the positive increase in C_{np} being larger than the destabilizing contribution of K_{XZ} . The effects of C_{np} on the damping of the lateral oscillation and aperiodic modes have been investigated in the past (refs. 13 and 14) where it was shown that positive increases in the derivative usually increases the damping of the Dutch roll mode while decreasing the damping of the roll-subsidence mode. The derivative C_{np} will almost always be increased positively by increasing vertical distance between the parawing and center of gravity. Increases in the same geometric variables will usually lead to negative values of K_{XZ} as explained previously.

It should be noted that in table III the contributions of $C_{n\beta}$, $C_{l\beta}$, and C_{lp} to the Dutch roll damping reverse signs between configurations A and B; that is, increases in the derivatives in the usual stabilizing sense (negative for C_{lp} , positive for $C_{n\beta}$ and $C_{l\beta}$) lead to less stable Dutch roll oscillations for configurations B and C. This result is due to the effect of C_{np} on the distribution of damping of the system. Similar results are reported in reference 13 for large positive values of C_{np} . As discussed in reference 14, the total damping of the system can be expressed as B/A . The partial derivative of the ratio with respect to any parameter x_i must therefore follow the relation

$$\frac{V}{0.693b} \frac{\partial B}{\partial x_i} = \left(\frac{\partial \frac{1}{t_{1/2}}}{\partial x_i} \right)_{\text{Spiral mode}} + \left(\frac{\partial \frac{1}{t_{1/2}}}{\partial x_i} \right)_{\text{Roll mode}} + 2 \left(\frac{\partial \frac{1}{t_{1/2}}}{\partial x_i} \right)_{\text{Dutch roll mode}}$$

Since $\frac{\partial B}{\partial x_i}$ for $C_{n\beta}$ and $C_{l\beta}$ must be zero (changes in these derivatives do not change the total damping but merely redistribute the damping among the modes), the stabilizing contribution of the derivatives to the roll-subsidence damping is accompanied by a decrease in the Dutch roll damping.

Theoretical investigations in the past (see ref. 15, for example) have shown that the

reversal of the sign of $\left(\frac{\partial \frac{1}{t_{1/2}}}{\partial C_{l\beta}} \right)_{\text{Dutch roll mode}}$ between configurations A and B could be predicted by the algebraic sign of the expression

$$C_{np} - 2C_L K_Z^2$$

Positive values of this quantity indicated that increases in the effective dihedral parameter $-C_{l\beta}$ would lead to larger values of the Dutch roll damping factor. The reversal of the sense of the contribution of $C_{l\beta}$ to the damping of the lateral oscillation as the center of gravity was lowered with respect to the parawing was therefore due to the positive increase in C_{np} brought about by center-of-gravity position.

The data presented in tables III and IV indicate that the decrease in frequency of the Dutch roll oscillation with increasing values of \bar{x}/b was due primarily to the mass parameters K_{XZ} and K_X^2 and the stability derivatives $C_{n\beta}$, C_{np} , and $C_{l\beta}$.

Although changes in lateral stability with center-of-gravity location have been discussed only for changes from that of configuration A to that of configuration B, similar results occur in going from configuration B to configuration C.

Lateral response to wing bank control.- The incremental lateral-force and moment coefficients presented in figure 9 indicate that as the center-of-gravity location was changed from that of configuration A to that of configuration C, the incremental rolling-moment coefficient ΔC_l increased as a result of the increased value of \bar{z}/b . The incremental yawing-moment coefficient ΔC_n is negative, or adverse, for all configurations. The responses of the configuration to 5° wing bank control are presented in figure 13. The results of the three-degree-of-freedom calculations show that the initial roll response was about equal for all configurations, but as the motion progressed, the configurations with the lower center-of-gravity locations (configurations B and C) showed greater response to wing bank control. The enlarged plot of the time history of the initial yawing motions shown in figure 14 indicates that increasing the vertical center-of-gravity location decreased the initial adverse yawing motion, which is opposite to what would be expected from a static aerodynamic standpoint. This result is caused by the favorable contribution of the product-of-inertia factor to the initial yawing acceleration as expressed by the relation:

$$D_b^2 \psi = \frac{\Delta C_n - \frac{K_{XZ}}{K_X^2} \Delta C_l}{2K_Z^2 \mu_b \left(1 - \frac{K_{XZ}^2}{K_X^2 K_Z^2} \right)} \quad (2)$$

As pointed out in reference 16 and as can be seen from equation (2), negative values of K_{XZ} give a favorable yawing-moment contribution and can thereby significantly affect the yawing characteristics in an aileron roll as the center-of-gravity location is lowered from that of configuration A to that of configuration C. The product-of-inertia parameter, as discussed earlier, will almost certainly be negative for large values of z/b .

SUMMARY OF RESULTS

The results of a theoretical investigation of the dynamic lateral stability and control of a parawing configuration having rigid leading edge and keel members may be summarized as follows:

1. Increasing the vertical distance between the center of gravity and the parawing keel while maintaining the horizontal location required for longitudinal trim led to a decrease in the damping of the roll-subsidence mode and an increase in the damping of the spiral mode. Lowering the center of gravity also caused an increase in the damping and period of the lateral oscillation and a reduction in the ratio of roll to sideslip.
2. The two parameters that most affected the damping of the lateral oscillation with vertical changes in center-of-gravity location were the yawing-moment-due-to-rolling derivative C_{np} and the nondimensional product-of-inertia factor K_{XZ} .
3. There was little effect of vertical center-of-gravity location on the initial roll response to wing bank control but as the motion progressed, the configurations having the lower centers of gravity displayed the greater roll response. The effects of vertical center-of-gravity location on the mass distribution of the system produced significant changes in the initial adverse yawing motion following the application of wing bank control. Negative values of K_{XZ} caused by lowering the center of gravity relative to the parawing tended to reduce the initial adverse yaw.

Langley Research Center,
National Aeronautics and Space Administration,
Langley Station, Hampton, Va., February 24, 1966.

APPENDIX A

STABILITY DERIVATIVE TRANSFER EQUATIONS

The stability derivative transfer equations given herein were taken from reference 7 and are expressed in the notation of this paper. The distances x and z correspond to those of figure 3. Zero subscripts indicate data measured about the basic reference center. The equations convert body-axis derivatives to stability-axis derivatives.

$$C_{Y\beta} = C_{Y\beta_0}$$

$$C_{Yp} = C_{Yp_0} \cos \alpha + C_{Yr_0} \sin \alpha + 2C_{Y\beta_0} \left(\frac{z}{b} \cos \alpha - \frac{x}{b} \sin \alpha \right)$$

$$C_{Yr} = C_{Yr_0} \cos \alpha - C_{Yp_0} \sin \alpha - 2C_{Y\beta_0} \left(\frac{x}{b} \cos \alpha + \frac{z}{b} \sin \alpha \right)$$

$$C_{l\beta} = C_{l\beta_0} \cos \alpha + C_{n\beta_0} \sin \alpha + C_{Y\beta} \left(\frac{z}{b} \cos \alpha - \frac{x}{b} \sin \alpha \right)$$

$$\begin{aligned} C_{lp} = & C_{lp_0} \cos^2 \alpha + (C_{lr_0} + C_{np_0}) \sin \alpha \cos \alpha + C_{nr_0} \sin^2 \alpha \\ & + \left[(C_{Yp_0} + 2C_{l\beta_0}) \cos \alpha + (C_{Yr_0} + 2C_{n\beta_0}) \sin \alpha \right] \left(\frac{z}{b} \cos \alpha - \frac{x}{b} \sin \alpha \right) \\ & + 2C_{Y\beta_0} \left(\frac{z}{b} \cos \alpha - \frac{x}{b} \sin \alpha \right)^2 \end{aligned}$$

$$\begin{aligned} C_{lr} = & C_{lr_0} \cos^2 \alpha + (C_{nr_0} - C_{lp_0}) \sin \alpha \cos \alpha - C_{np_0} \sin^2 \alpha \\ & - \frac{x}{b} \left[2C_{l\beta_0} \cos^2 \alpha + (C_{Yr_0} + 2C_{n\beta_0}) \sin \alpha \cos \alpha - C_{Yp_0} \sin^2 \alpha \right] \\ & + \frac{z}{b} \left[C_{Yr_0} \cos^2 \alpha - (C_{Yp_0} + 2C_{l\beta_0}) \sin \alpha \cos \alpha - 2C_{n\beta_0} \sin^2 \alpha \right] \\ & + 2C_{Y\beta_0} \left[\left(\frac{x^2}{b^2} - \frac{z^2}{b^2} \right) \sin \alpha \cos \alpha - \frac{xz}{b} (\cos^2 \alpha - \sin^2 \alpha) \right] \end{aligned}$$

APPENDIX A

$$C_{n\beta} = C_{n\beta_0} \cos \alpha - C_{l\beta_0} \sin \alpha - C_{Y\beta_0} \left(\frac{x}{b} \cos \alpha + \frac{z}{b} \sin \alpha \right)$$

$$\begin{aligned} C_{np} &= C_{np_0} \cos^2 \alpha + (C_{nr_0} - C_{lp_0}) \sin \alpha \cos \alpha - C_{lr_0} \sin^2 \alpha \\ &\quad - \frac{x}{b} \left[C_{Yp_0} \cos^2 \alpha + (C_{Yr_0} + 2C_{n\beta_0}) \sin \alpha \cos \alpha - 2C_{l\beta_0} \sin^2 \alpha \right] \\ &\quad + \frac{z}{b} \left[2C_{n\beta_0} \cos^2 \alpha - (C_{Yp_0} + 2C_{l\beta_0}) \sin \alpha \cos \alpha - C_{Yr_0} \sin^2 \alpha \right] \\ &\quad + 2C_{Y\beta_0} \left[\left(\frac{x^2}{b^2} - \frac{z^2}{b^2} \right) \sin \alpha \cos \alpha - \frac{xz}{b^2} (\cos^2 \alpha - \sin^2 \alpha) \right] \end{aligned}$$

$$\begin{aligned} C_{nr} &= C_{nr_0} \cos^2 \alpha - (C_{lr_0} + C_{np_0}) \sin \alpha \cos \alpha + C_{lp_0} \sin^2 \alpha \\ &\quad - \left[(C_{Yr_0} + 2C_{n\beta_0}) \cos \alpha - (C_{Yp_0} + 2C_{l\beta_0}) \sin \alpha \right] \left(+ \frac{x}{b} \cos \alpha + \frac{z}{b} \sin \alpha \right) \\ &\quad + 2C_{Y\beta_0} \left(- \frac{x}{b} \cos \alpha - \frac{z}{b} \sin \alpha \right)^2 \end{aligned}$$

APPENDIX B

EQUATIONS OF MOTION

The nondimensional lateral equations of motion (ref. 13), referred to a stability axis system (fig. 1), are:

Roll:

$$2\mu_b \left(K_X^2 D_b^2 \phi + K_{XZ} D_b^2 \psi \right) = C_{l_\beta} \beta + \frac{1}{2} C_{l_p} D_b \phi + \frac{1}{2} C_{l_r} D_b \psi$$

Yaw:

$$2\mu_b \left(K_Z^2 D_b^2 \psi + K_{XZ} D_b^2 \phi \right) = C_{n_\beta} \beta + \frac{1}{2} C_{n_p} D_b \phi + \frac{1}{2} C_{n_r} D_b \psi$$

Sideslip:

$$2\mu_b \left(D_b \beta + D_b \psi \right) = C_{Y_\beta} \beta + \frac{1}{2} C_{Y_p} D_b \phi + C_L \phi + \frac{1}{2} C_{Y_r} D_b \psi + \left(C_L \tan \gamma \right) \psi$$

When $\phi_0 e^{\lambda s_b}$ is substituted for ϕ , $\psi_0 e^{\lambda s_b}$ for ψ , and $\beta_0 e^{\lambda s_b}$ for β in the equations written in determinant form, λ must be a root of the stability equation (neglecting the zero or heading root)

$$A\lambda^4 + B\lambda^3 + C\lambda^2 + D\lambda + E = 0 \quad (B1)$$

where

$$A = 8\mu_b^3 \left(K_X^2 K_Z^2 - K_{XZ}^2 \right)$$

$$B = -2\mu_b^2 \left(2K_X^2 K_Z^2 C_{Y_\beta} + K_X^2 C_{n_r} + K_Z^2 C_{l_p} - 2K_{XZ}^2 C_{Y_\beta} - K_{XZ} C_{l_r} - K_{XZ} C_{n_p} \right)$$

$$C = \mu_b \left(K_X^2 C_{n_r} C_{Y_\beta} + 4\mu_b K_X^2 C_{n_\beta} + K_Z^2 C_{l_p} C_{Y_\beta} + \frac{1}{2} C_{n_r} C_{l_p} - K_{XZ} C_{l_r} C_{Y_\beta} - 4\mu_b K_{XZ} C_{l_\beta} \right. \\ \left. - C_{n_p} K_{XZ} C_{Y_\beta} - \frac{1}{2} C_{n_p} C_{l_r} + K_{XZ} C_{n_\beta} C_{Y_p} - K_Z^2 C_{Y_p} C_{l_\beta} - K_X^2 C_{Y_r} C_{n_\beta} + K_{XZ} C_{Y_r} C_{l_\beta} \right)$$

APPENDIX B

$$\begin{aligned}
 D = & -\frac{1}{4} C_{nr} C_{lp} C_{Y\beta} - \mu_b C_{lp} C_{n\beta} + \frac{1}{4} C_{np} C_{lr} C_{Y\beta} + \mu_b C_{np} C_{l\beta} + 2\mu_b C_L K_{XZ} C_{n\beta} \\
 & - 2\mu_b C_L K_Z^2 C_{l\beta} - 2\mu_b K_X^2 C_{n\beta} C_L \tan \gamma + 2\mu_b K_{XZ} C_L C_L \tan \gamma + \frac{1}{4} C_{lp} C_{n\beta} C_{Yr} \\
 & - \frac{1}{4} C_{np} C_{l\beta} C_{Yr} - \frac{1}{4} C_{lr} C_{n\beta} C_{Yp} + \frac{1}{4} C_{nr} C_{l\beta} C_{Yp}
 \end{aligned}$$

$$E = \frac{1}{2} C_L (C_{nr} C_{l\beta} - C_{lr} C_{n\beta}) + \frac{1}{2} C_L \tan \gamma (C_{lp} C_{n\beta} - C_{np} C_{l\beta})$$

The damping and period of a mode of motion in seconds are given, respectively, by the equations $t_{1/2} = -\frac{0.69}{c} \frac{b}{V}$ and $P = \frac{2\pi}{d} \frac{b}{V}$ where c and d are the real and imaginary parts of the root of the stability equation.

REFERENCES

1. Shanks, Robert E.: Experimental Investigation of the Dynamic Stability of a Towed Parawing Glider Air Cargo Delivery System. NASA TN D-2292, 1964.
2. Burk, Sanger, M., Jr.: Free-Flight Investigation of the Deployment, Dynamic Stability, and Control Characteristics of a 1/12-Scale Dynamic Radio-Controlled Model of a Large Booster and Parawing. NASA TN D-1932, 1963.
3. Johnson, Joseph L., Jr.: Low-Speed Force and Flight Investigation of a Model of a Modified Parawing Utility Vehicle. NASA TN D-2492, 1965.
4. Hewes, Donald E.: Free-Flight Investigation of Radio-Controlled Models With Parawings. NASA TN D-927, 1961.
5. Polhamus, Edward C.; and Naeseth, Rodger L.: Experimental and Theoretical Studies of the Effects of Camber and Twist on the Aerodynamic Characteristics of Parawings Having Nominal Aspect Ratios of 3 and 6. NASA TN D-972, 1963.
6. Hewes, Donald E.: Low-Subsonic Measurements of the Static and Oscillatory Lateral Stability Derivatives of a Sweptback-Wing Airplane Configuration at Angles of Attack From -10° to 90° . NASA MEMO 5-20-59L, 1959.
7. Babister, A. W.: Aircraft Stability and Control. Pergamon Press, c.1961.
8. Gates, Ordway, Jr.; and Woodling, C. H.: A Method for Estimating Variations in the Roots of the Lateral-Stability Quartic Due to Changes in Mass and Aerodynamic Parameters of an Airplane. NACA TN 3134, 1954.
9. Moul, Martin T.; and Paulson, John W.: Dynamic Lateral Behavior of High-Performance Aircraft. NACA RM L58E16, 1958.
10. Campbell, John P.; Johnson, Joseph L., Jr.; and Hewes, Donald E.: Low-Speed Study of the Effect of Frequency on the Stability Derivatives of Wings Oscillating in Yaw With Particular Reference to High Angle-of-Attack Conditions. NACA RM L55H05, 1955.
11. Anon.: Flying Qualities of Piloted Airplanes. MIL-F-8785 (ASG), Sept. 1, 1954; Amendment-4, Apr. 17, 1959.
12. Anon.: Flying Qualities of Piloted Airplanes. USAF Spec. No. 1815-B, June 1, 1948.
13. Johnson, Joseph L.; and Sternfield, Leonard: A Theoretical Investigation of the Effect of Yawing Moment Due to Rolling on Lateral Oscillatory Stability. NACA TN 1723, 1948.

14. Schade, Robert O.; and Hassell, James L., Jr.: The Effects on Dynamic Lateral Stability and Control of Large Artificial Variations in the Rotary Stability Derivatives. NACA Rept. 1151, 1953. (Supersedes NACA TN 2781.)
15. Sternfield, Leonard; and Gates, Ordway B., Jr.: A Simplified Method for the Determination and Analysis of the Neutral-Lateral Stability Boundary. NACA Rept. 943, 1949. (Supersedes NACA TN 1727.)
16. Hewes, Donald E.: The Effects of Mass Distribution on the Low-Speed Dynamic Lateral Stability and Control Characteristics of a Model With a 45° Sweptback Wing. NACA TN 2313, 1951.

TABLE I.- GEOMETRIC CHARACTERISTICS OF THE MODEL

Aspect ratio:	
Flat	2.83
Deployed	2.57
Area:	
Flat	1.14 sq m (12.27 sq ft)
Deployed	1.04 sq m (11.16 sq ft)
Mean aerodynamic chord:	
Flat and deployed	84.6 cm (33.33 in.)
Span:	
Flat	179 cm (70.71 in.)
Deployed	163 cm (64.28 in.)
Root chord	127 cm (50.00 in.)
Sweep angle:	
Flat	45.00 deg
Deployed	50.00 deg

TABLE II.- MASS AND AERODYNAMIC PARAMETERS OF THE CONFIGURATIONS

[All values are presented with respect to stability axes]

Parameter	Configuration		
	A	B	C
$C_{Y\beta}$	-0.2556	-0.2556	-0.2556
$C_{n\beta}$	0.072165	0.082705	0.09325
$C_{l\beta}$	-0.14287	-0.208458	-0.27405
C_{Yp}	0.0701	-0.06107	-0.1923
C_{Yr}	0.00314	0.02422	0.04529
C_{lp}	-0.08946	-0.17846	-0.33479
C_{lr}	0.03054	0.04852	0.07725
C_{np}	0.009	0.0486	0.09898
C_{nr}	-0.01757	-0.02452	-0.0332
K_X^2	0.01815	0.04118	0.079694
K_Z^2	0.0163	0.01697	0.018045
K_{XZ}	0.000681	-0.003266	-0.00972
μ_b	3.183	3.183	3.183
C_L	0.757	0.757	0.757
$\tan \gamma$	-0.2338	-0.2338	-0.2338
η	$-18^{\circ}12'$	$7^{\circ}36'$	$9^{\circ}12'$
x/b	-0.0636	-0.1348	-0.2060
z/b	0.25	0.50	0.75

TABLE III.- VARIATION OF THE LATERAL STABILITY OF THE THREE CONFIGURATIONS
WITH CHANGES IN THE STABILITY PARAMETERS

x_i	Spiral $\frac{\partial}{\partial x_i} \frac{1}{t_{1/2}}$	Roll subsidence	Dutch roll	
		$\frac{\partial}{\partial x_i} \frac{1}{t_{1/2}}$	$\frac{\partial}{\partial x_i} \frac{1}{t_{1/2}}$	$\frac{\partial \omega}{\partial x_i}$
Configuration A				
C_{lp}	-0.24	-14.059	-0.97	-0.13
C_{np}	-0.47	-20.82	11.012	-4.88
C_{yp}	0.00021	-0.18	0.091	0.11
C_{lr}	-3.77	3.36	0.55	0.20
C_{nr}	-7.45	4.97	-7.81	1.46
C_{yr}	0.0034	0.043	-0.023	-0.079
$C_{l\beta}$	-0.67	-1.23	0.95	-0.83
$C_{n\beta}$	-1.32	-1.82	1.56	13.88
$C_{y\beta}$	0.00059	-0.016	-0.29	0.0034
$\gamma \dot{\beta}$	-0.25	-0.089	0.17	-0.017
$K_{X\dot{\beta}}$	-0.062	-85.36	1.87	-7.63
$K_{Z\dot{\beta}}$	-1.92	30.18	-24.81	-60.69
$K_{XZ\dot{\beta}}$	-1.091	-106.045	77.57	89.41
Configuration B				
C_{lp}	-0.029	-9.22	0.10	-0.11
C_{np}	-0.074	-21.34	10.011	-2.56
C_{yp}	0.000023	-0.099	0.050	0.089
C_{lr}	-4.26	4.55	-0.84	0.013
C_{nr}	-10.74	10.52	-8.70	1.32
C_{yr}	0.0034	0.049	-0.026	-0.078
$C_{l\beta}$	-0.95	2.052	-0.55	1.51
$C_{n\beta}$	-2.38	4.65	-1.13	16.35
$C_{y\beta}$	0.00076	0.022	-0.31	-0.0042
$\gamma \dot{\beta}$	-0.17	-0.50	0.33	-0.044
$K_{X\dot{\beta}}$	-0.010	-33.83	2.54	6.65
$K_{Z\dot{\beta}}$	-3.69	38.61	-26.91	-57.82
$K_{XZ\dot{\beta}}$	-1.49	-61.62	44.78	59.82
Configuration C				
C_{lp}	0.29	-6.57	1.12	0.096
C_{np}	0.86	-18.88	7.95	-0.86
C_{yp}	-0.00017	-0.046	0.023	0.066
C_{lr}	-5.36	5.93	-1.36	-0.16
C_{nr}	-15.74	17.064	-9.39	0.73
C_{yr}	0.0026	0.042	-0.022	-0.079
$C_{l\beta}$	-1.77	5.15	-1.69	2.32
$C_{n\beta}$	-5.13	14.48	-4.68	17.50
$C_{y\beta}$	0.00092	0.035	-0.35	-0.0091
$\gamma \dot{\beta}$	0.019	-1.045	0.51	-0.027
$K_{X\dot{\beta}}$	0.13	-14.43	0.52	7.45
$K_{Z\dot{\beta}}$	-6.89	37.49	-23.94	-58.095
$K_{XZ\dot{\beta}}$	-1.97	-28.45	23.58	39.97

TABLE IV.- VARIATION OF THE LATERAL STABILITY OF CONFIGURATION A
WITH CHANGES IN THE STABILITY PARAMETERS*

K_X^2	K_Z^2	K_{XZ}	$C_{l\beta}$	$C_{n\beta}$	C_{Yp}	C_{lp}	C_{np}	C_{Yr}	C_{lr}	C_{nr}	Spiral	Roll subsidence	Dutch roll	
											$\Delta \frac{1}{t_{1/2}}$	$\Delta \frac{1}{t_{1/2}}$	$\Delta\omega$	$\Delta \frac{1}{t_{1/2}}$
<u>0.04118</u>	0.01630	0.00068	-0.14287	0.07216	0.07010	-0.08946	0.00900	0.00314	0.03054	-0.01757	-0.0014 (-.0014)	-0.93 (-1.97)	-0.081 (-.18)	0.059 (.043)
.01815	<u>.01697</u>	.00068	-.14287	.07216	.07010	-.08946	.00900	.00314	.03054	-.01757	-.0013 (-.0013)	.020 (.020)	-.039 (-.041)	-.016 (-.017)
.01815	.01630	<u>-.00327</u>	-.14287	.07216	.07010	-.08946	.00900	.00314	.03054	-.01757	.0045 (.0043)	.51 (.42)	-.30 (-.35)	-.31 (-.31)
.01815	.01630	.00068	<u>-.20846</u>	.07216	.07010	-.08946	.00900	.00314	.03054	-.01757	.040 (.044)	.078 (.081)	.054 (.055)	-.059 (-.062)
.01815	.01630	.00068	-.14287	<u>.08271</u>	.07010	-.08946	.00900	.00314	.03054	-.01757	-.013 (-.014)	-.018 (-.019)	.14 (.15)	.015 (.016)
.01815	.01630	.00068	-.14287	.07216	<u>-.06107</u>	-.08946	.00900	.00314	.03054	-.01757	-.000037 (-.000028)	.024 (.024)	-.015 (-.015)	-.012 (-.012)
.01815	.01630	.00068	-.14287	.07216	.07010	<u>-.17846</u>	.00900	.00314	.03054	-.01757	.012 (.021)	1.29 (1.25)	-.0046 (.011)	.073 (.086)
.01815	.01630	.00068	-.14287	.07216	.07010	-.08946	<u>.04860</u>	.00314	.03054	-.01757	-.051 (-.019)	-1.02 (-.83)	-.15 (-.19)	.55 (.44)
.01815	.01630	.00068	-.14287	.07216	.07010	-.08946	.00900	<u>.02422</u>	.03054	-.01757	.000062 (.000070)	.00072 (.00092)	-.0017 (-.0017)	-.00050 (-.00049)
.01815	.01630	.00068	-.14287	.07216	.07010	-.08946	.00900	.00314	<u>.04852</u>	-.01757	-.065 (-.068)	.058 (.060)	.0036 (.0036)	.0097 (.0098)
.01815	.01630	.00068	-.14287	.07216	.07010	-.08946	.00900	.00314	.03054	<u>-.02452</u>	.053 (.051)	-.037 (-.035)	-.011 (-.010)	.054 (.054)

*Derivatives changed one at a time to the values for configuration B. Derivatives changed are underlined. Variations predicted by the slope method of reference 8 are indicated in parentheses.

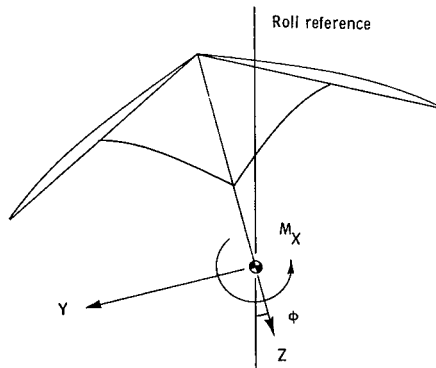
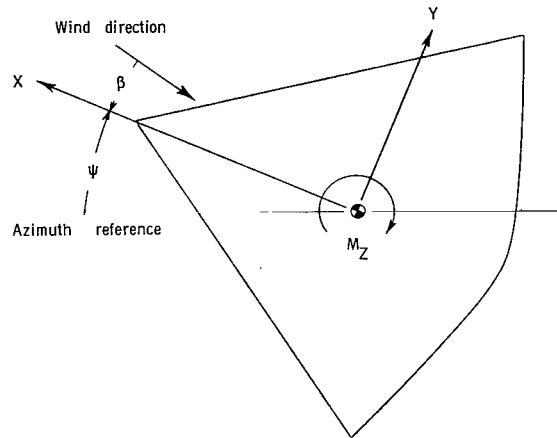
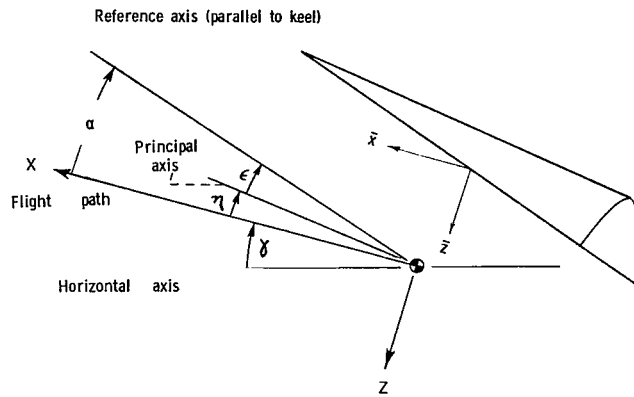


Figure 1.- The stability system of axes. Arrows indicate positive directions of moments, forces, and angles. This system of axes is defined as an orthogonal system having the origin at the center of gravity and in which the Z-axis is in the plane of symmetry and perpendicular to the relative wind, the X-axis is in the plane of symmetry and perpendicular to the Z-axis, and the Y-axis is perpendicular to the plane of symmetry. At a constant angle of attack, these axes are fixed in the configuration.

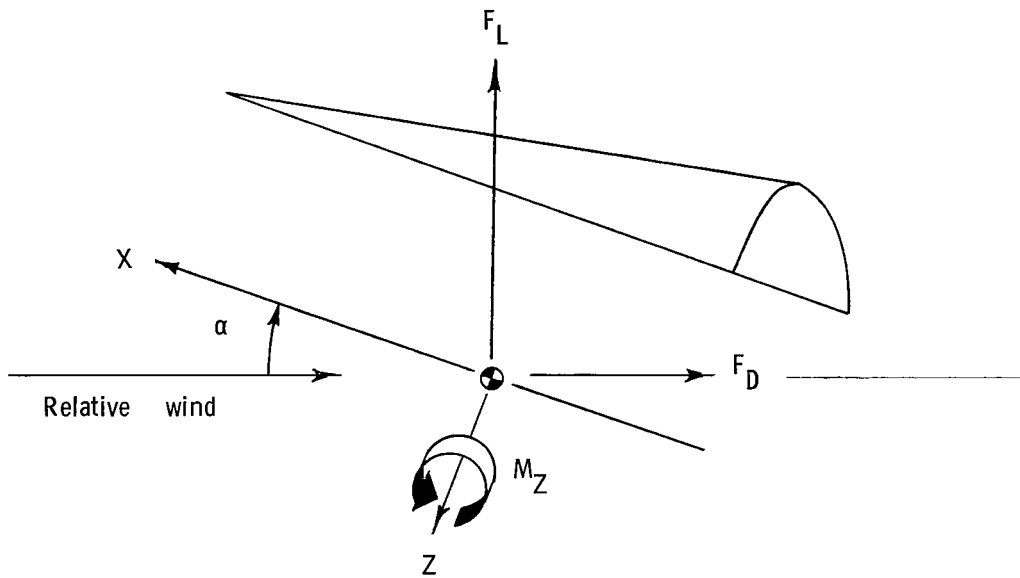
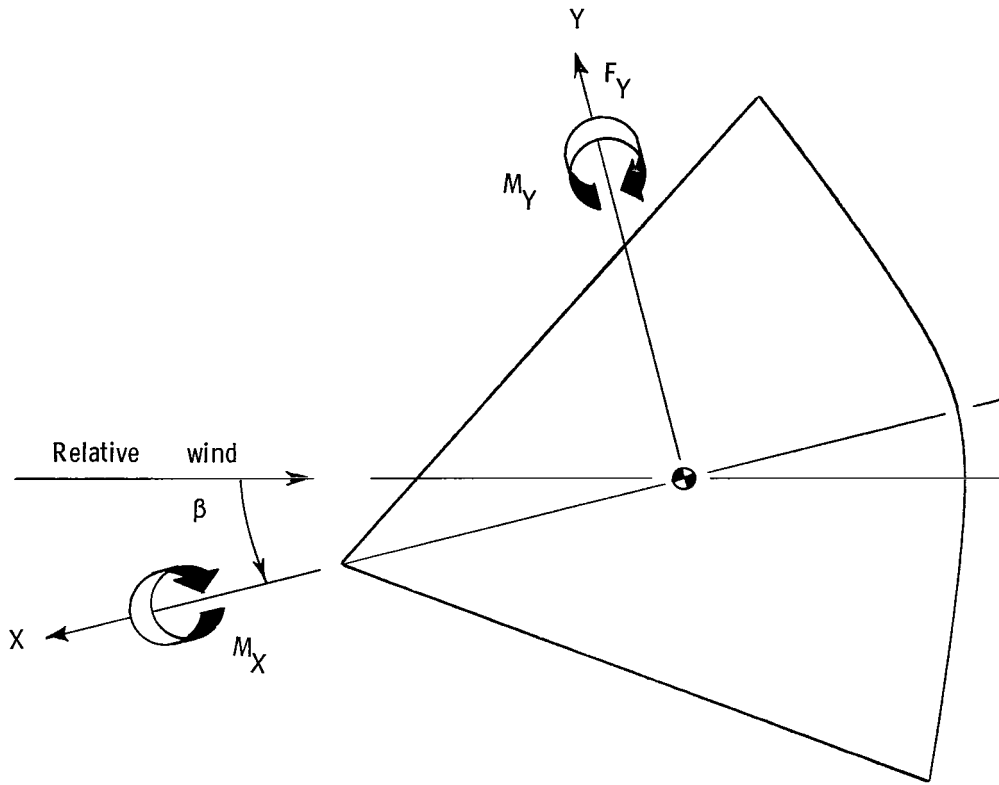


Figure 2.- Sketch of the body axis system. The X-axis is located in the plane of symmetry and parallel to the keel member, the Z-axis is in the plane of symmetry and perpendicular to the keel member, and the Y-axis is perpendicular to the plane of symmetry.

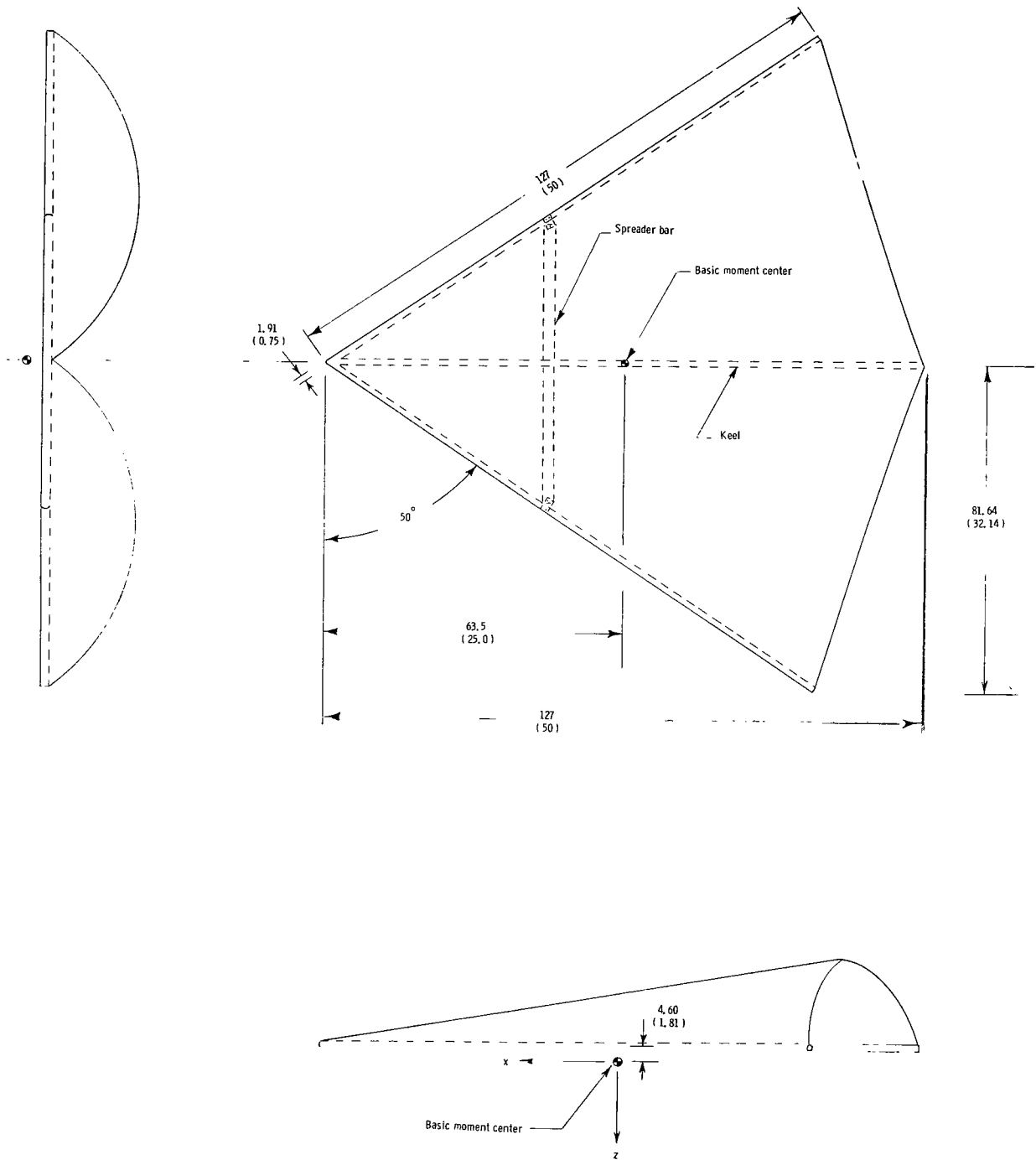


Figure 3.- Geometry of the deployed model. Dimensions are given first in centimeters, then parenthetically in inches.

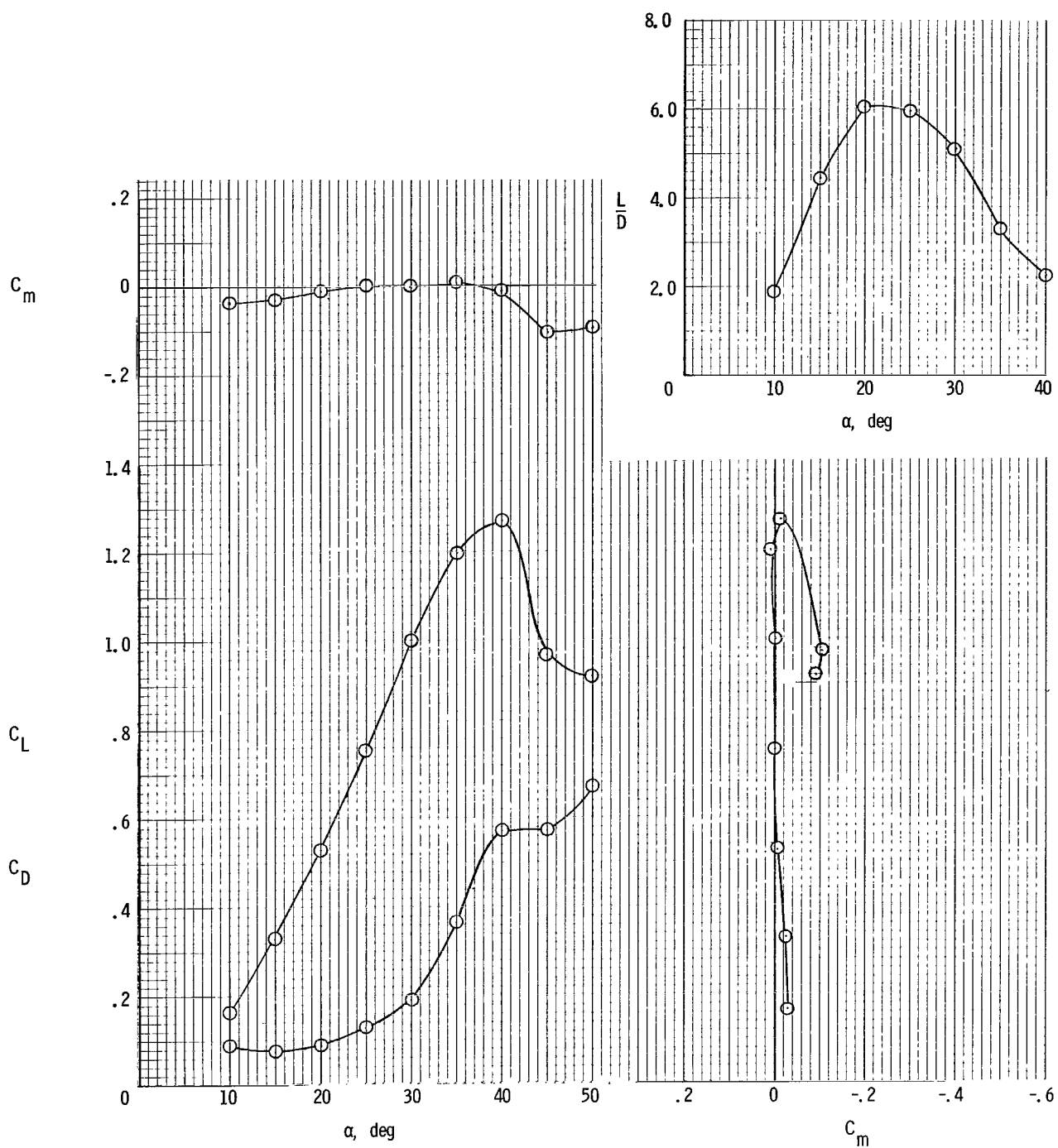


Figure 4.- Summary of the static longitudinal characteristics of the 0.15-scale model parawing.

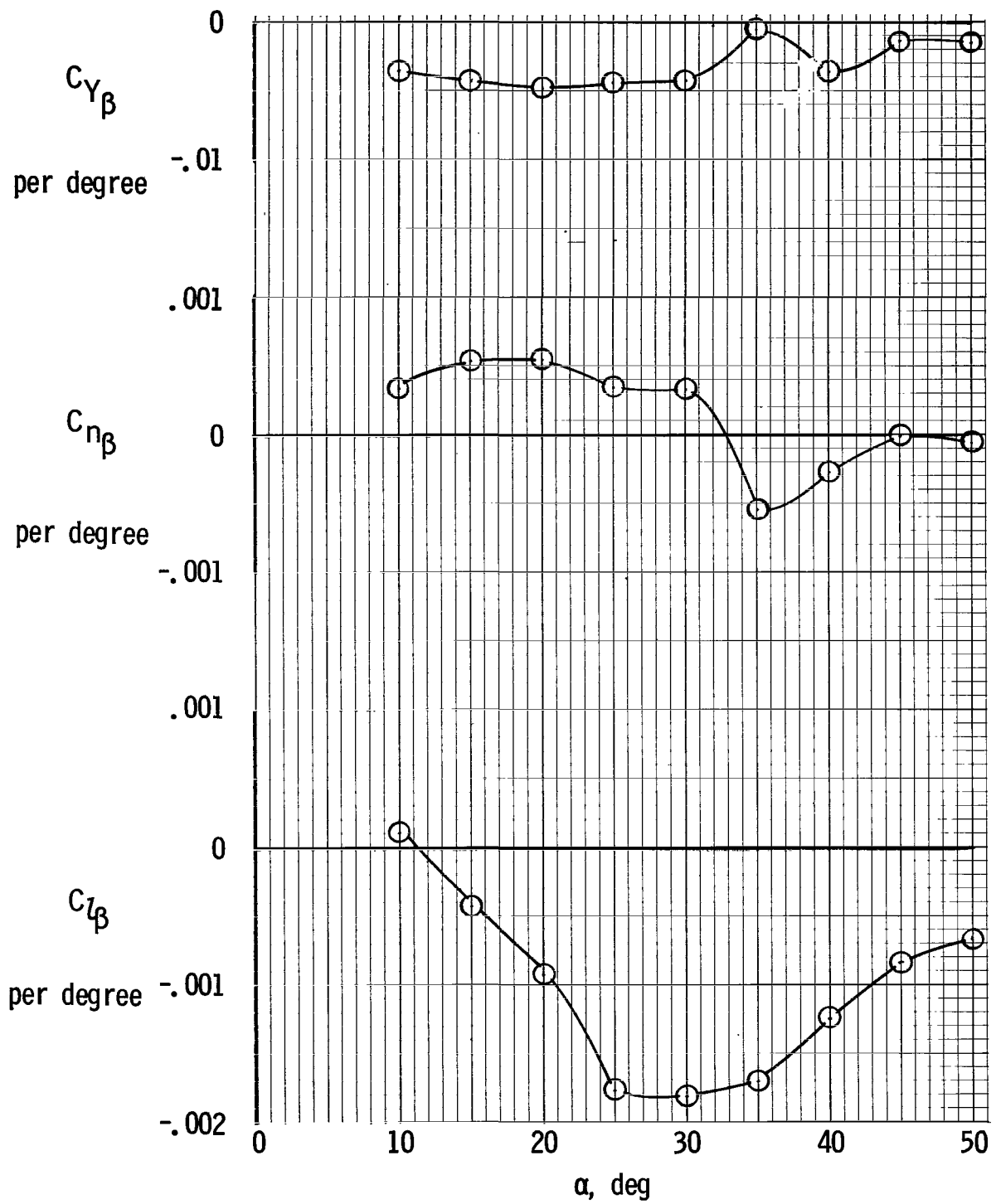
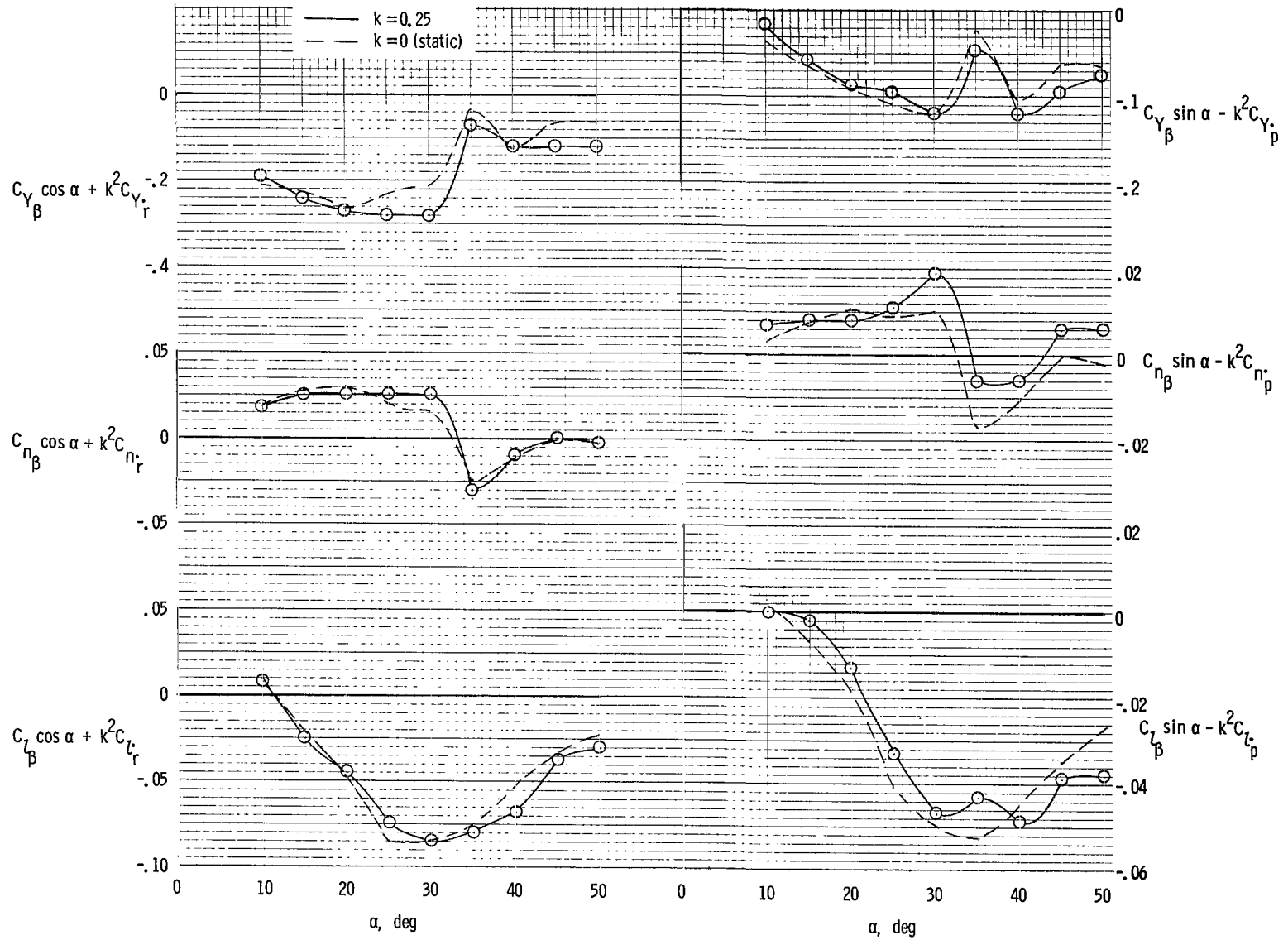


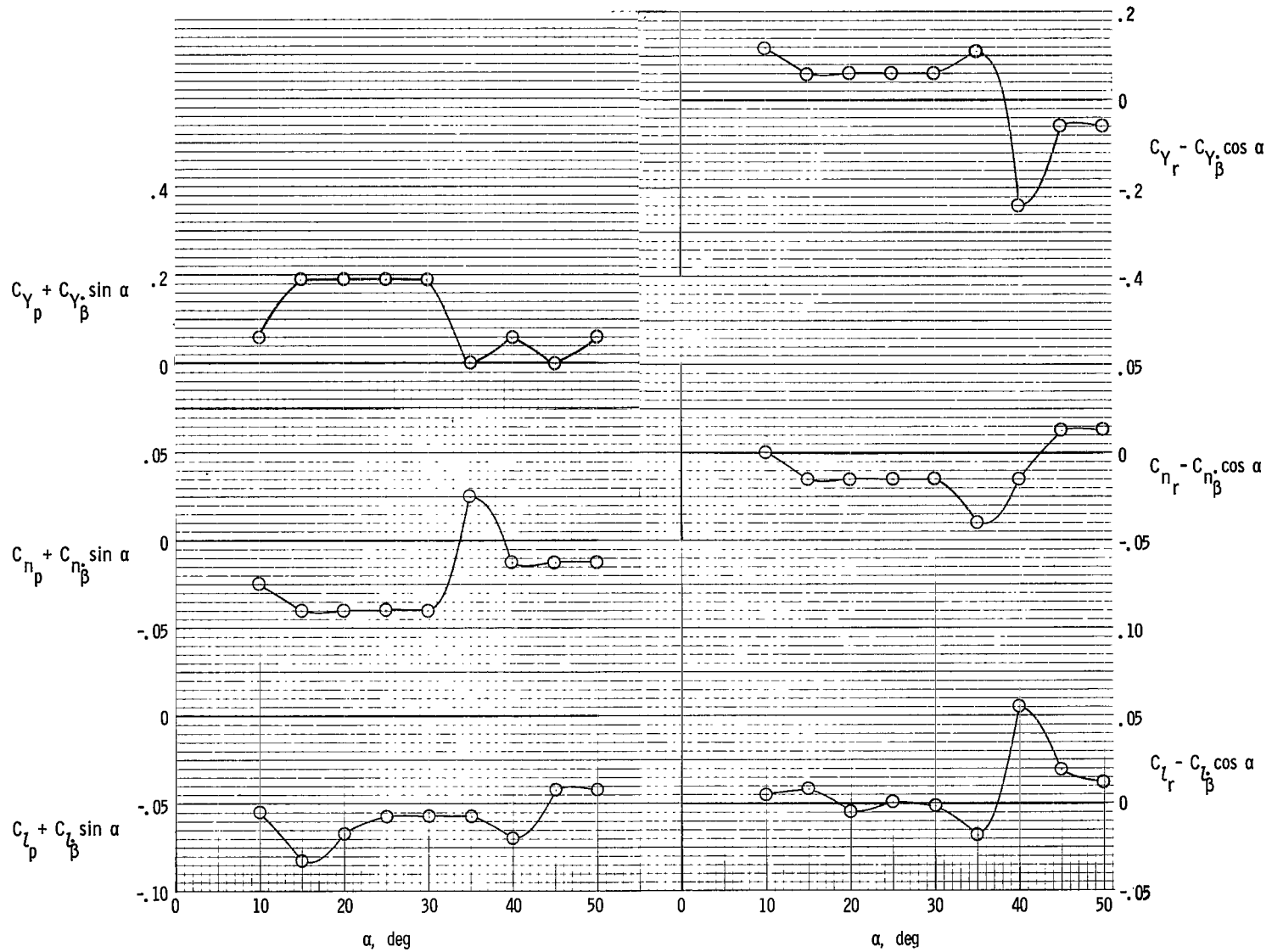
Figure 5.- Variation of the static lateral stability derivatives of the 0.15-scale model with angle of attack. Data referenced to body axes.



(a) Yawing.

(b) Rolling.

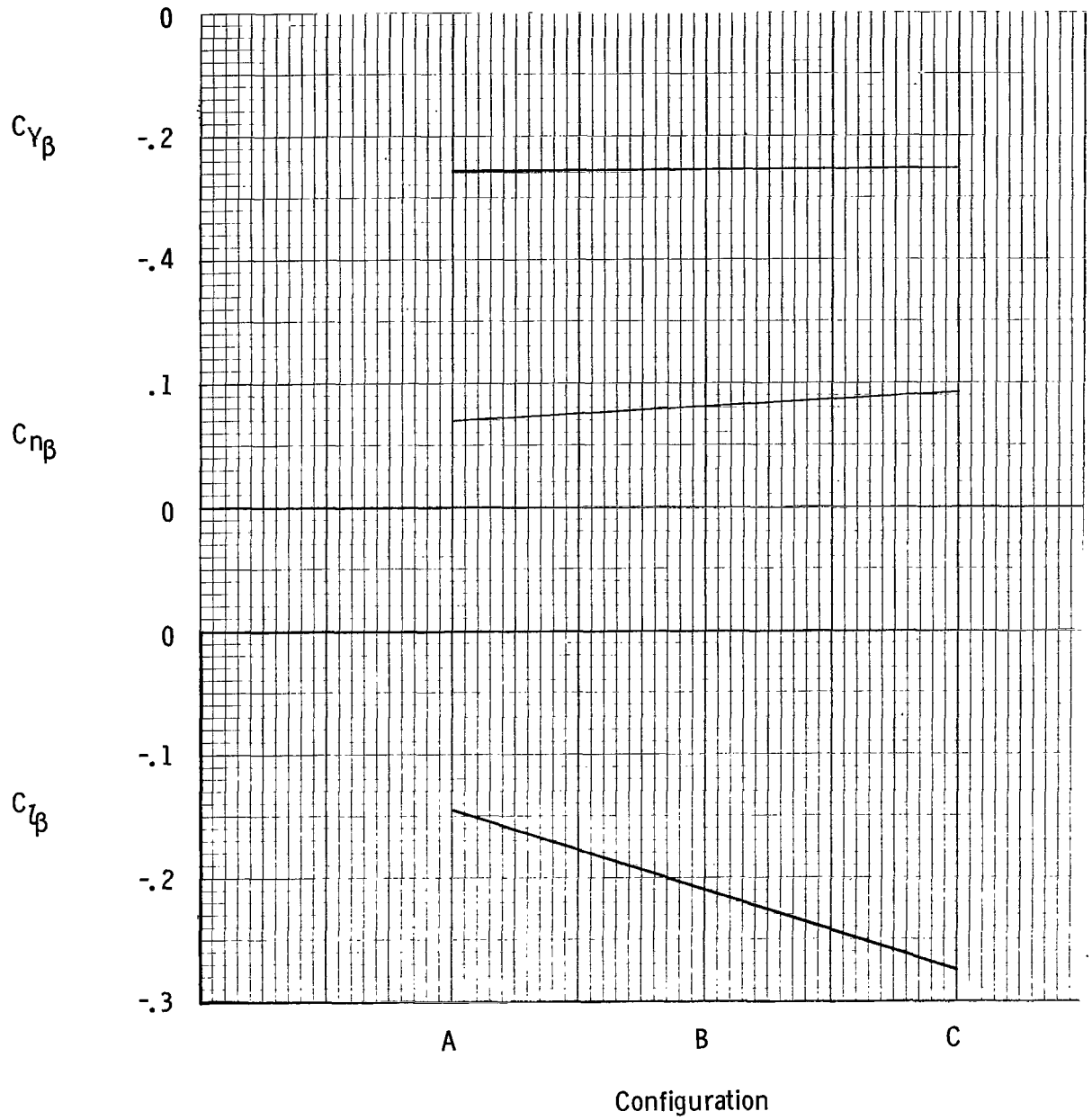
Figure 6.- Variation of the lateral in-phase oscillatory derivatives with angle of attack. Data referenced to body axes.



(a) Rolling.

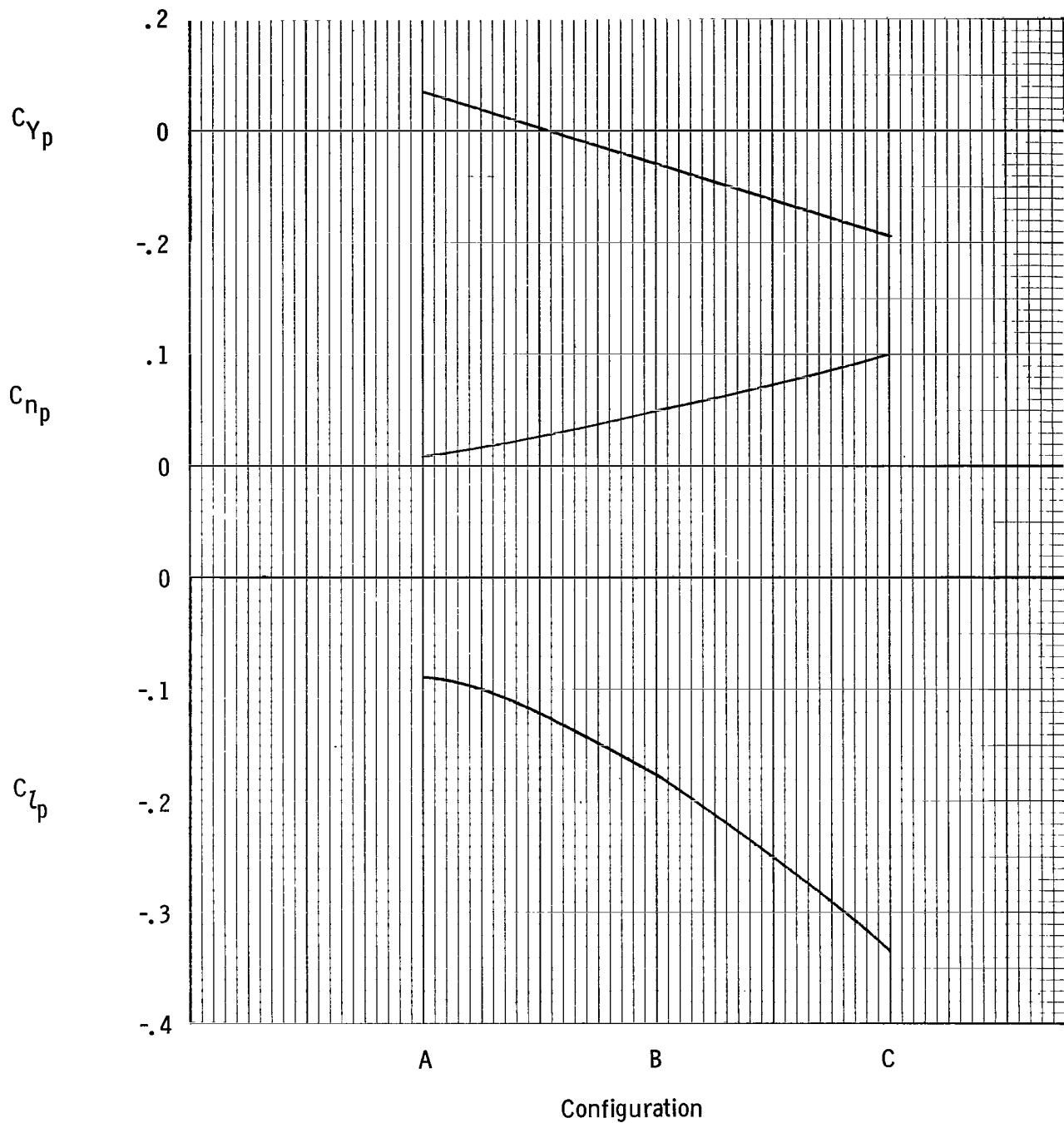
(b) Yawing.

Figure 7.- Variation of the lateral out-of-phase oscillatory derivatives with angle of attack. Data referenced to body axes.



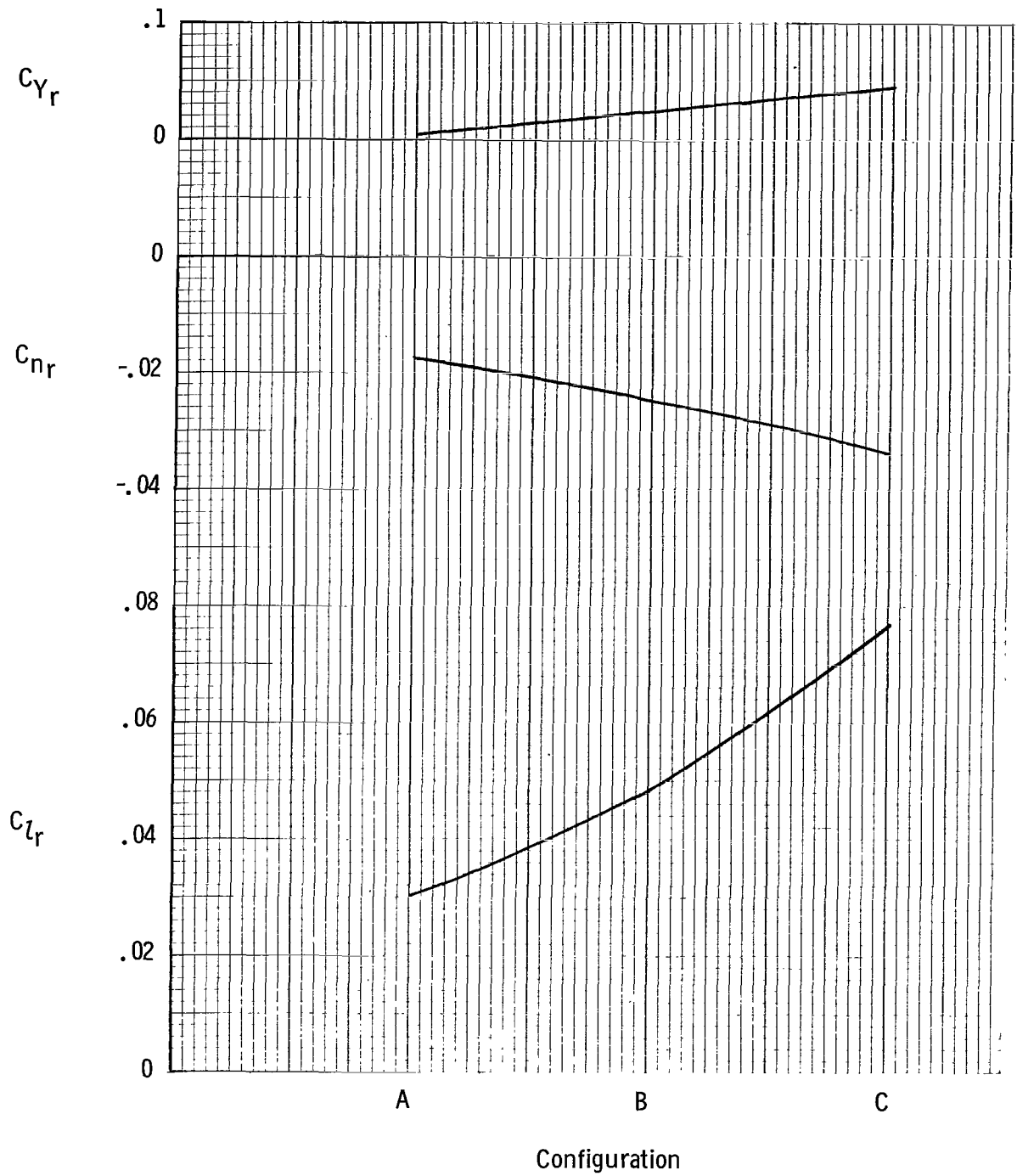
(a) Static lateral derivatives.

Figure 8.- Variation of the lateral stability derivatives with the three center-of-gravity locations. Data referenced to stability axes; $\alpha = 25^\circ$.



(b) Rolling derivatives.

Figure 8.- Continued.



(c) Yawing derivatives.

Figure 8.- Concluded.

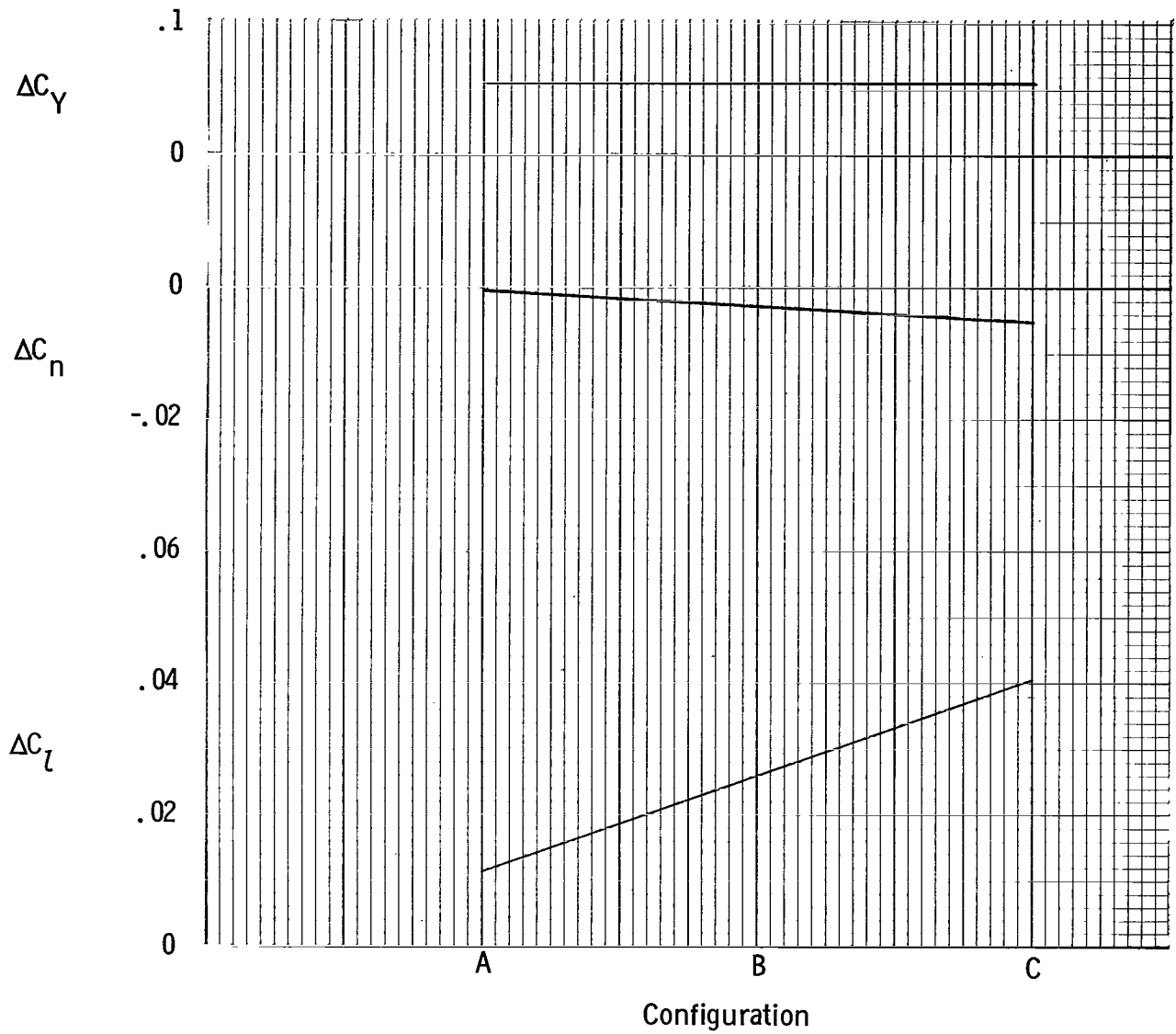


Figure 9.- Incremental values of lateral-force and moment coefficients for the three configurations caused by 5° wing bank angle. Data referenced to stability axes; $\alpha = 25^\circ$.

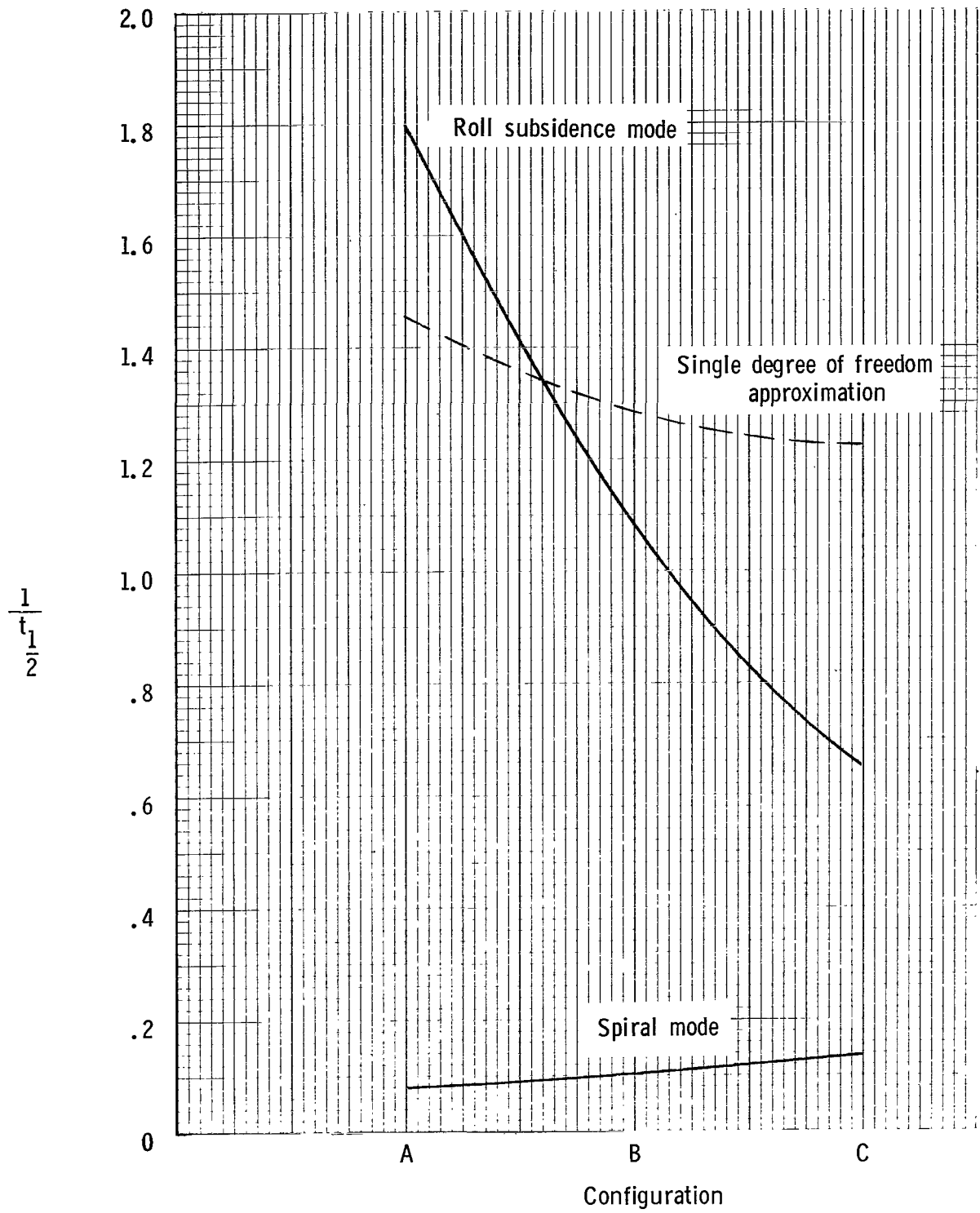


Figure 10.- Variation of the damping factor of the lateral aperiodic modes with center-of-gravity location.

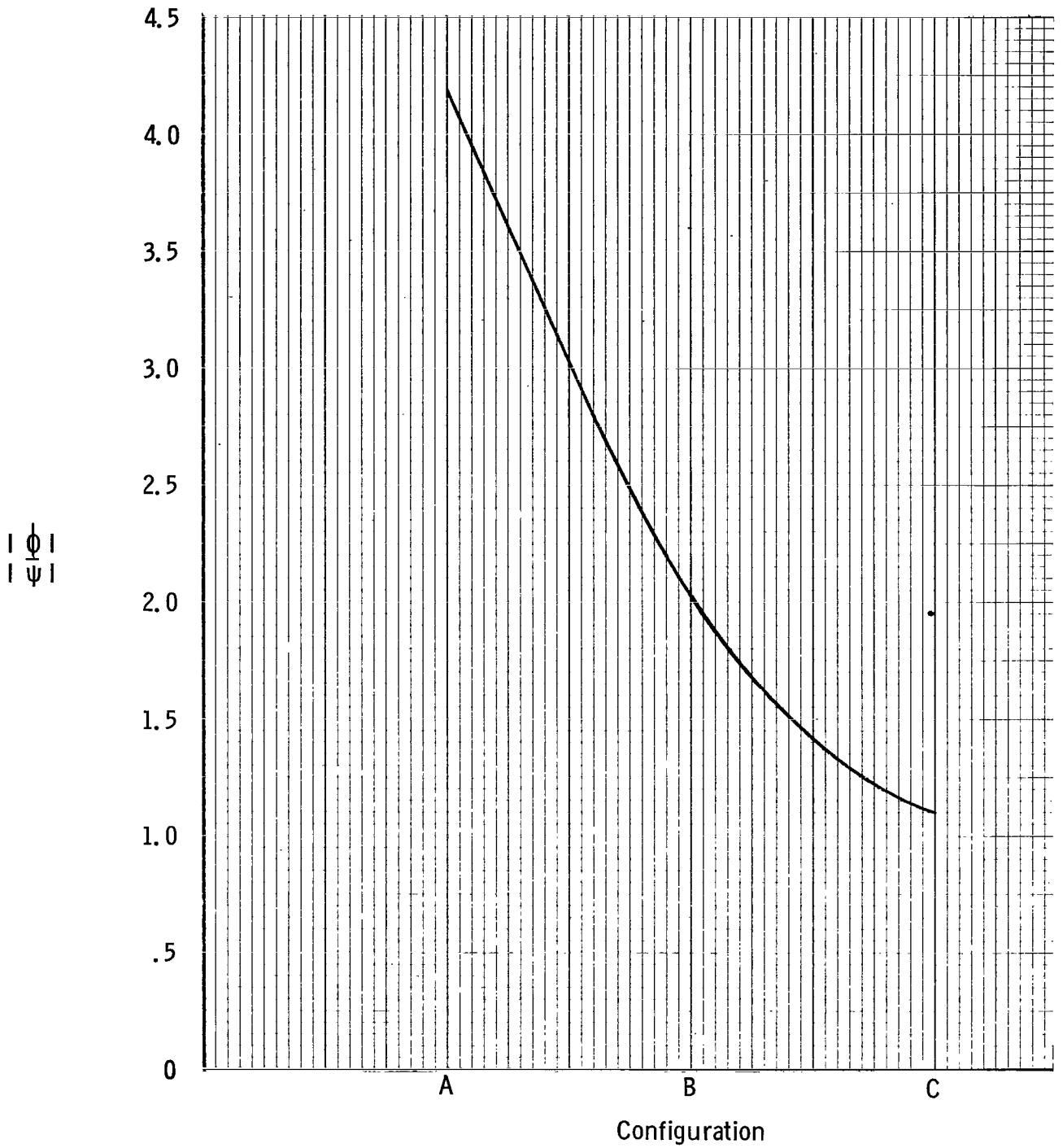
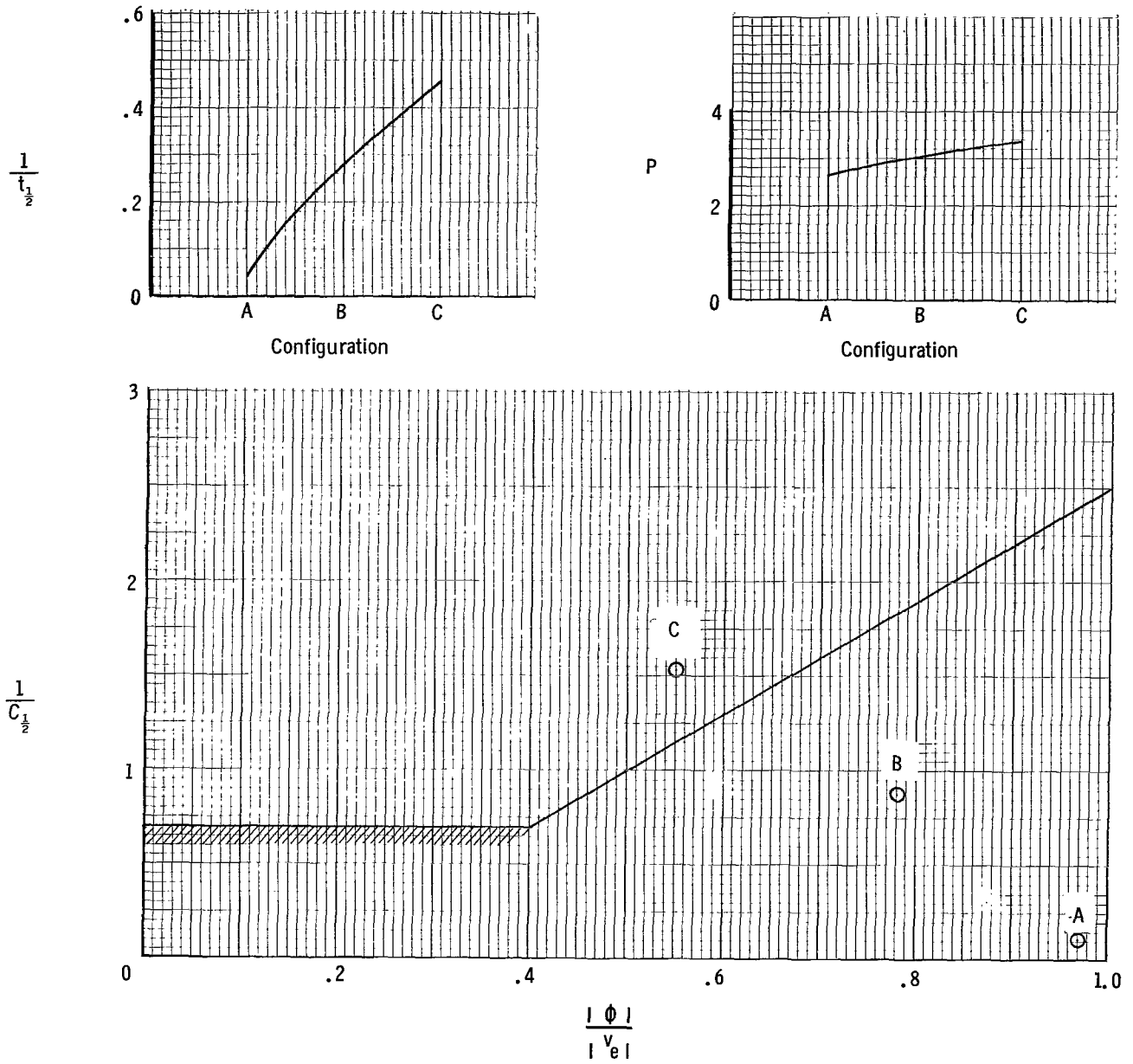
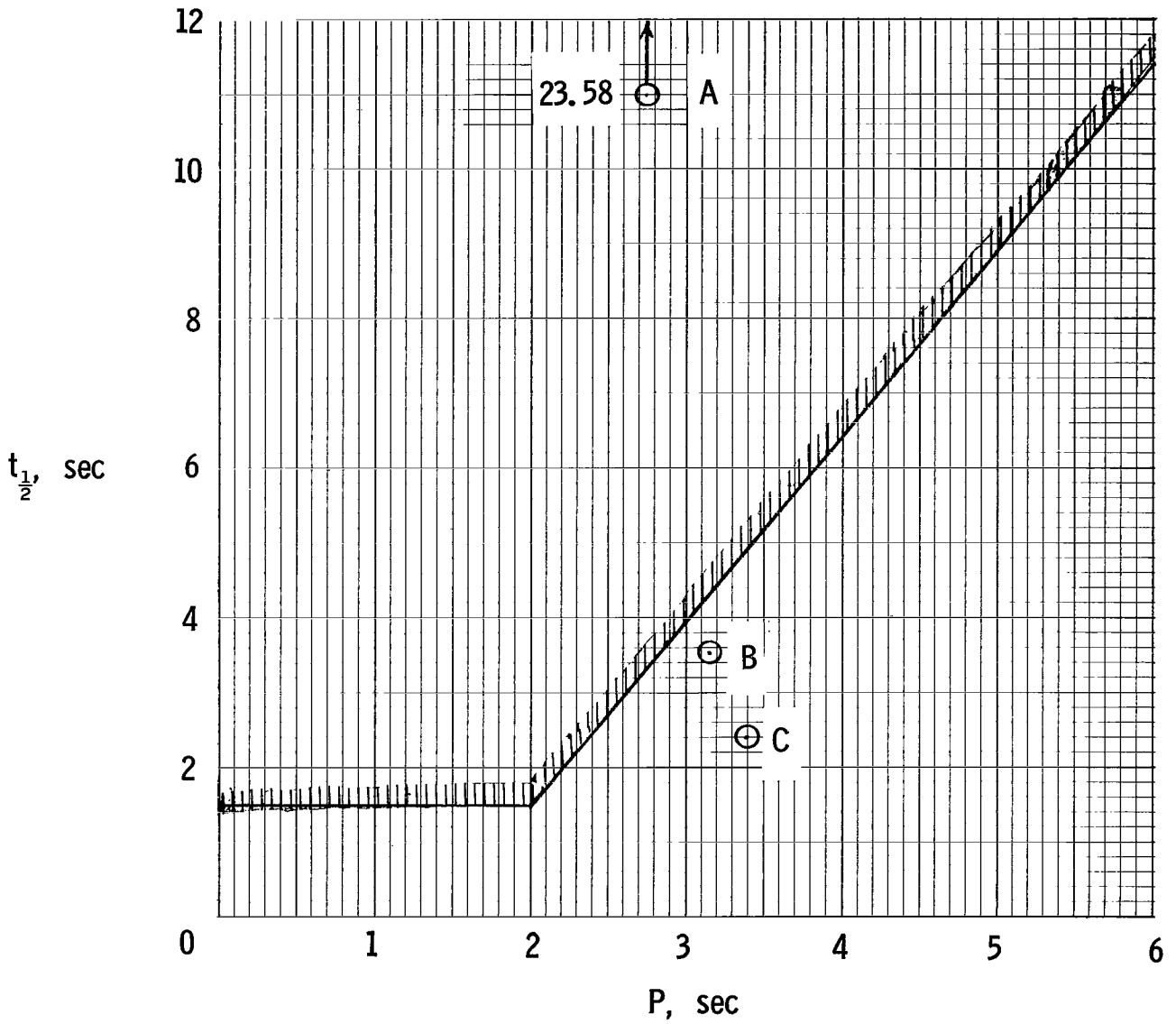


Figure 11.- Variation of the roll-yaw ratio of the roll-subsidence mode with center-of-gravity location.



(a) Compared with requirements of reference 11.

Figure 12.- Summary of the variation of the lateral oscillatory characteristics with center-of-gravity location.



(b) Compared with requirements of reference 12.

Figure 12.- Concluded.

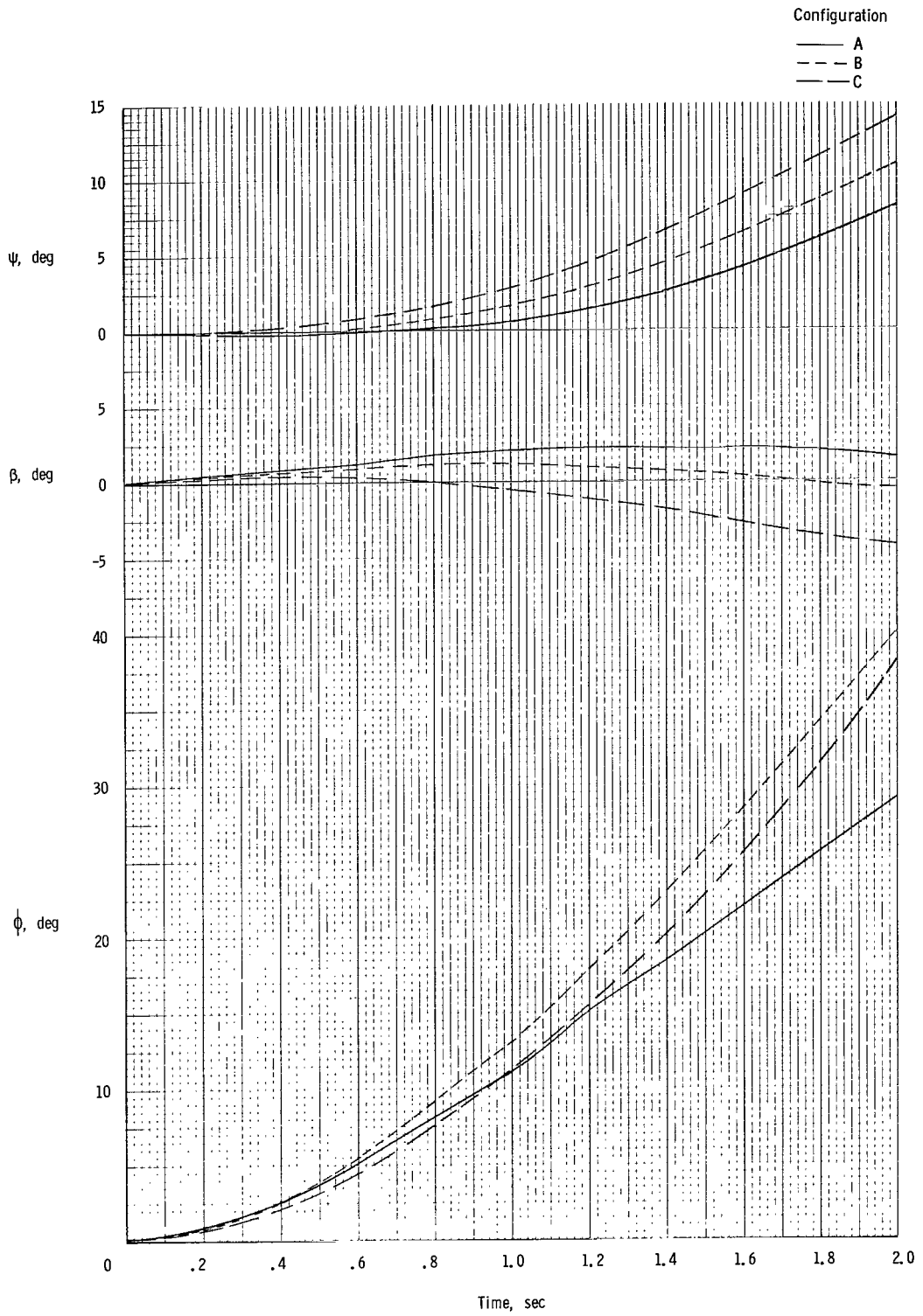


Figure 13.- Effect of center-of-gravity location on lateral response to wing bank control. $\Phi_W = 5^\circ$.

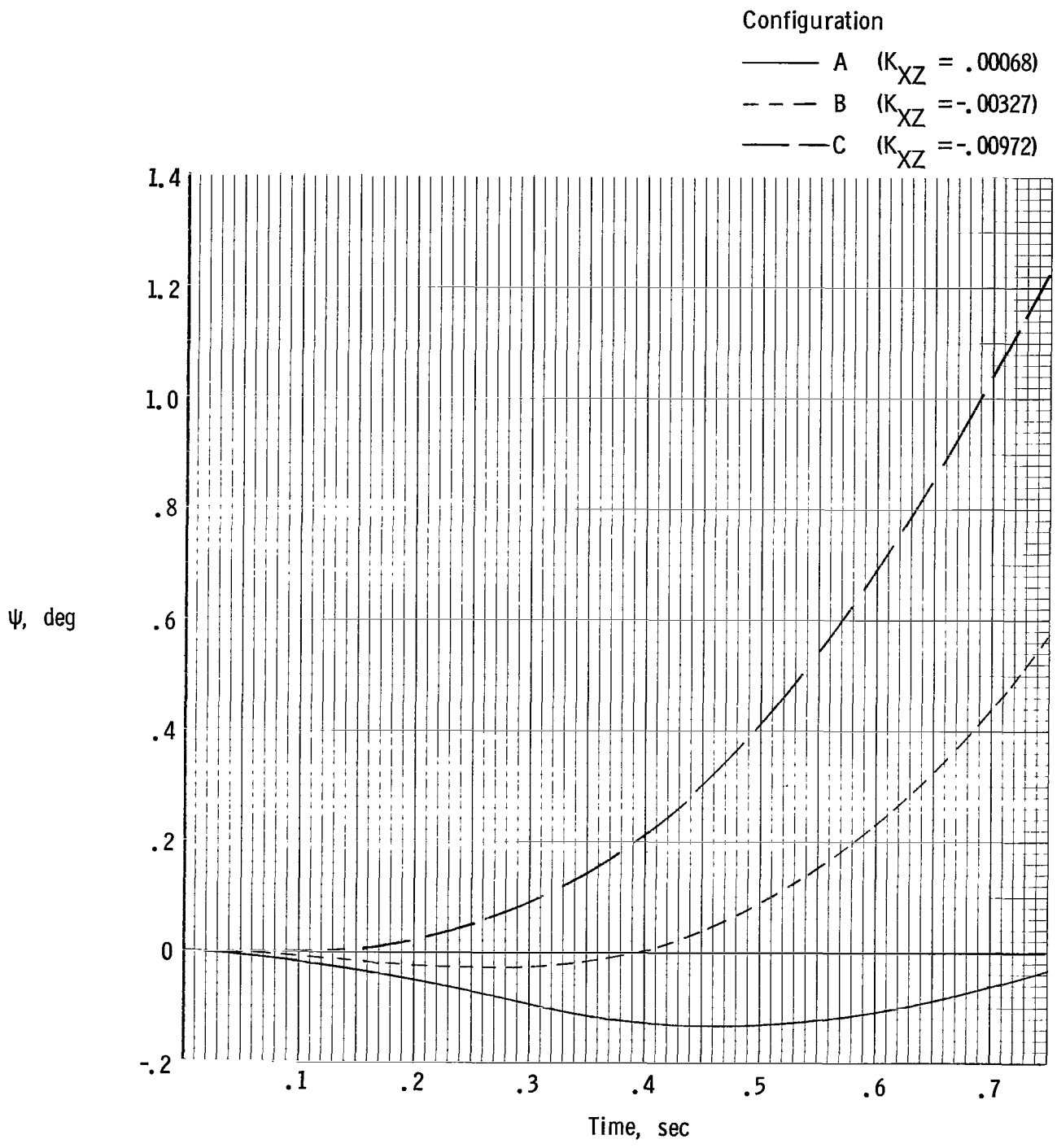


Figure 14.- Effect of center-of-gravity location on initial yawing motion of lateral response.

"The aeronautical and space activities of the United States shall be conducted so as to contribute . . . to the expansion of human knowledge of phenomena in the atmosphere and space. The Administration shall provide for the widest practicable and appropriate dissemination of information concerning its activities and the results thereof."

—NATIONAL AERONAUTICS AND SPACE ACT OF 1958

NASA SCIENTIFIC AND TECHNICAL PUBLICATIONS

TECHNICAL REPORTS: Scientific and technical information considered important, complete, and a lasting contribution to existing knowledge.

TECHNICAL NOTES: Information less broad in scope but nevertheless of importance as a contribution to existing knowledge.

TECHNICAL MEMORANDUMS: Information receiving limited distribution because of preliminary data, security classification, or other reasons.

CONTRACTOR REPORTS: Technical information generated in connection with a NASA contract or grant and released under NASA auspices.

TECHNICAL TRANSLATIONS: Information published in a foreign language considered to merit NASA distribution in English.

TECHNICAL REPRINTS: Information derived from NASA activities and initially published in the form of journal articles.

SPECIAL PUBLICATIONS: Information derived from or of value to NASA activities but not necessarily reporting the results of individual NASA-programmed scientific efforts. Publications include conference proceedings, monographs, data compilations, handbooks, sourcebooks, and special bibliographies.

Details on the availability of these publications may be obtained from:

SCIENTIFIC AND TECHNICAL INFORMATION DIVISION
NATIONAL AERONAUTICS AND SPACE ADMINISTRATION
Washington, D.C. 20546